

1

Emulsion Formation, Stability, and Rheology

Tharwat F. Tadros

1.1

Introduction

Emulsions are a class of disperse systems consisting of two immiscible liquids [1–3]. The liquid droplets (the disperse phase) are dispersed in a liquid medium (the continuous phase). Several classes may be distinguished: oil-in-water (O/W), water-in-oil (W/O), and oil-in-oil (O/O). The latter class may be exemplified by an emulsion consisting of a polar oil (e.g., propylene glycol) dispersed in a nonpolar oil (paraffinic oil) and vice versa. To disperse two immiscible liquids, one needs a third component, namely, the emulsifier. The choice of the emulsifier is crucial in the formation of the emulsion and its long-term stability [1–3].

Emulsions may be classified according to the nature of the emulsifier or the structure of the system. This is illustrated in Table 1.1.

1.1.1

Nature of the Emulsifier

The simplest type is ions such as OH^- that can be specifically adsorbed on the emulsion droplet thus producing a charge. An electrical double layer can be produced, which provides electrostatic repulsion. This has been demonstrated with very dilute O/W emulsions by removing any acidity. Clearly that process is not practical. The most effective emulsifiers are nonionic surfactants that can be used to emulsify O/W or W/O. In addition, they can stabilize the emulsion against flocculation and coalescence. Ionic surfactants such as sodium dodecyl sulfate (SDS) can also be used as emulsifiers (for O/W), but the system is sensitive to the presence of electrolytes. Surfactant mixtures, for example, ionic and nonionic, or mixtures of nonionic surfactants can be more effective in emulsification and stabilization of the emulsion. Nonionic polymers, sometimes referred to as *polymeric surfactants*, for example, Pluronic, are more effective in stabilization of the emulsion, but they may suffer from the difficulty of emulsification (to produce small droplets) unless high energy is applied for the process. Polyelectrolytes such as poly(methacrylic

Table 1.1 Classification of emulsion types.

Nature of emulsifier	Structure of the system
Simple molecules and ions	Nature of internal and external phase: O/W, W/O
Nonionic surfactants	—
Surfactant mixtures	Micellar emulsions (microemulsions)
Ionic surfactants	Macroemulsions
Nonionic polymers	Bilayer droplets
Polyelectrolytes	Double and multiple emulsions
Mixed polymers and surfactants	Mixed emulsions
Liquid crystalline phases	—
Solid particles	—

acid) can also be applied as emulsifiers. Mixtures of polymers and surfactants are ideal in achieving ease of emulsification and stabilization of the emulsion. Lamellar liquid crystalline phases that can be produced using surfactant mixtures are very effective in emulsion stabilization. Solid particles that can accumulate at the O/W interface can also be used for emulsion stabilization. These are referred to as *Pickering emulsions*, whereby particles are made partially wetted by the oil phase and by the aqueous phase.

1.1.2

Structure of the System

- 1) **O/W and W/O macroemulsions:** These usually have a size range of 0.1–5 μm with an average of 1–2 μm .
- 2) **Nanoemulsions:** these usually have a size range of 20–100 nm. Similar to macroemulsions, they are only kinetically stable.
- 3) **Micellar emulsions or microemulsions:** these usually have the size range of 5–50 nm. They are thermodynamically stable.
- 4) **Double and multiple emulsions:** these are emulsions-of-emulsions, W/O/W, and O/W/O systems.
- 5) **Mixed emulsions:** these are systems consisting of two different disperse droplets that do not mix in a continuous medium. This chapter only deals with macroemulsions.

Several breakdown processes may occur on storage depending on particle size distribution and density difference between the droplets and the medium. Magnitude of the attractive versus repulsive forces determines flocculation. Solubility of the disperse droplets and the particle size distribution determine Ostwald ripening. Stability of the liquid film between the droplets determines coalescence. The other process is phase inversion.

1.1.3

Breakdown Processes in Emulsions

The various breakdown processes are illustrated in Figure 1.1. The physical phenomena involved in each breakdown process are not simple, and it requires analysis of the various surface forces involved. In addition, the above-mentioned processes may take place simultaneously rather than consecutively and this complicates the analysis. Model emulsions, with monodisperse droplets, cannot be easily produced, and hence, any theoretical treatment must take into account the effect of droplet size distribution. Theories that take into account the polydispersity of the system are complex, and in many cases, only numerical solutions are possible. In addition, measurements of surfactant and polymer adsorption in an emulsion are not easy and one has to extract such information from measurement at a planer interface.

In the following sections, a summary of each of the above-mentioned breakdown processes and details of each process and methods of its prevention are given.

1.1.4

Creaming and Sedimentation

This process results from external forces usually gravitational or centrifugal. When such forces exceed the thermal motion of the droplets (Brownian motion), a concentration gradient builds up in the system with the larger droplets moving faster to the top (if their density is lower than that of the medium) or to the bottom (if their density is larger than that of the medium) of the container. In the limiting cases, the droplets may form a close-packed (random or ordered) array at the top or bottom of the system with the remainder of the volume occupied by the continuous liquid phase.

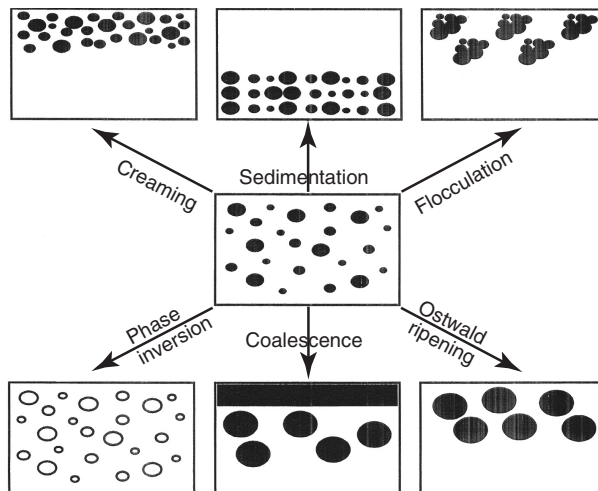


Figure 1.1 Schematic representation of the various breakdown processes in emulsions.

1.1.5

Flocculation

This process refers to aggregation of the droplets (without any change in primary droplet size) into larger units. It is the result of the van der Waals attraction that is universal with all disperse systems. Flocculation occurs when there is not sufficient repulsion to keep the droplets apart to distances where the van der Waals attraction is weak. Flocculation may be “strong” or “weak,” depending on the magnitude of the attractive energy involved.

1.1.6

Ostwald Ripening (Disproportionation)

This results from the finite solubility of the liquid phases. Liquids that are referred to as *being immiscible* often have mutual solubilities that are not negligible. With emulsions, which are usually polydisperse, the smaller droplets will have larger solubility when compared with the larger ones (due to curvature effects). With time, the smaller droplets disappear and their molecules diffuse to the bulk and become deposited on the larger droplets. With time, the droplet size distribution shifts to larger values.

1.1.7

Coalescence

This refers to the process of thinning and disruption of the liquid film between the droplets with the result of fusion of two or more droplets into larger ones. The limiting case for coalescence is the complete separation of the emulsion into two distinct liquid phases. The driving force for coalescence is the surface or film fluctuations which results in close approach of the droplets whereby the van der Waals forces is strong thus preventing their separation.

1.1.8

Phase Inversion

This refers to the process whereby there will be an exchange between the disperse phase and the medium. For example, an O/W emulsion may with time or change of conditions invert to a W/O emulsion. In many cases, phase inversion passes through a transition state whereby multiple emulsions are produced.

1.2

Industrial Applications of Emulsions

Several industrial systems consist of emulsions of which the following is worth mentioning: food emulsion, for example, mayonnaise, salad creams, deserts, and

beverages; personal care and cosmetics, for example, hand creams, lotions, hair sprays, and sunscreens; agrochemicals, for example, self-emulsifiable oils which produce emulsions on dilution with water, emulsion concentrates (EWs), and crop oil sprays; pharmaceuticals, for example, anesthetics of O/W emulsions, lipid emulsions, and double and multiple emulsions; and paints, for example, emulsions of alkyd resins and latex emulsions. Dry cleaning formulations – this may contain water droplets emulsified in the dry cleaning oil which is necessary to remove soils and clays. Bitumen emulsions: these are emulsions prepared stable in the containers, but when applied the road chippings, they must coalesce to form a uniform film of bitumen. Emulsions in the oil industry: many crude oils contain water droplets (for example, the North sea oil) and these must be removed by coalescence followed by separation. Oil slick dispersions: the oil spilled from tankers must be emulsified and then separated. Emulsification of unwanted oil: this is an important process for pollution control.

The above importance of emulsion in industry justifies a great deal of basic research to understand the origin of instability and methods to prevent their break down. Unfortunately, fundamental research on emulsions is not easy because model systems (e.g., with monodisperse droplets) are difficult to produce. In many cases, theories on emulsion stability are not exact and semiempirical approaches are used.

1.3 Physical Chemistry of Emulsion Systems

1.3.1 The Interface (Gibbs Dividing Line)

An interface between two bulk phases, for example, liquid and air (or liquid/vapor), or two immiscible liquids (oil/water) may be defined provided that a dividing line is introduced (Figure 1.2). The interfacial region is not a layer that is one-molecule thick. It is a region with thickness δ with properties different from the two bulk phases α and β .

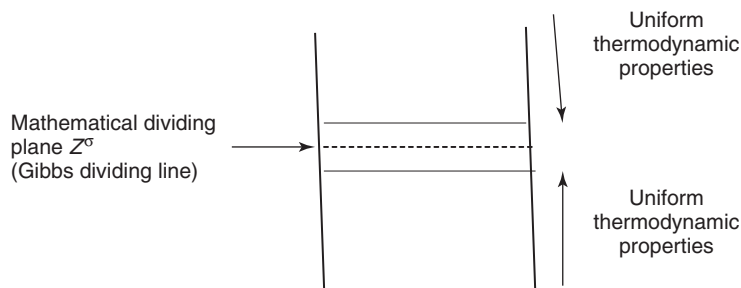


Figure 1.2 The Gibbs dividing line.

Using Gibbs model, it is possible to obtain a definition of the surface or interfacial tension γ .

The surface free energy dG^σ is made of three components: an entropy term $S^\sigma dT$, an interfacial energy term $Ad\gamma$, and a composition term $\sum n_i d\mu_i$ (n_i is the number of moles of component i with chemical potential μ_i). The Gibbs–Deuhem equation is

$$dG^\sigma = -S^\sigma dT + Ad\gamma + \sum n_i d\mu_i \quad (1.1)$$

At constant temperature and composition

$$\begin{aligned} dG^\sigma &= Ad\gamma \\ \gamma &= \left(\frac{\partial G^\sigma}{\partial A} \right)_{T, n_i} \end{aligned} \quad (1.2)$$

For a stable interface, γ is positive, that is, if the interfacial area increases G^σ increases. Note that γ is energy per unit area (mJ m^{-2}), which is dimensionally equivalent to force per unit length (mN m^{-1}), the unit usually used to define surface or interfacial tension.

For a curved interface, one should consider the effect of the radius of curvature. Fortunately, γ for a curved interface is estimated to be very close to that of a planer surface, unless the droplets are very small (<10 nm). Curved interfaces produce some other important physical phenomena that affect emulsion properties, for example, the Laplace pressure Δp , which is determined by the radii of curvature of the droplets

$$\Delta p = \gamma \left(\frac{1}{r_1} + \frac{1}{r_2} \right) \quad (1.3)$$

where r_1 and r_2 are the two principal radii of curvature.

For a perfectly spherical droplet, $r_1 = r_2 = r$ and

$$\Delta p = \frac{2\gamma}{r} \quad (1.4)$$

For a hydrocarbon droplet with radius 100 nm, and $\gamma = 50$ mN m^{-1} , $\Delta p = 10^6$ Pa (10 atm).

1.4

Thermodynamics of Emulsion Formation and Breakdown

Consider a system in which an oil is represented by a large drop 2 of area A_1 immersed in a liquid 2, which is now subdivided into a large number of smaller droplets with total area A_2 ($A_2 \gg A_1$) as shown in Figure 1.3. The interfacial tension γ_{12} is the same for the large and smaller droplets because the latter are generally in the region of 0.1 to few micrometers.

The change in free energy in going from state I to state II is made from two contributions: A surface energy term (that is positive) that is equal to $\Delta A\gamma_{12}$ (where $\Delta A = A_2 - A_1$). An entropy of dispersions term that is also positive

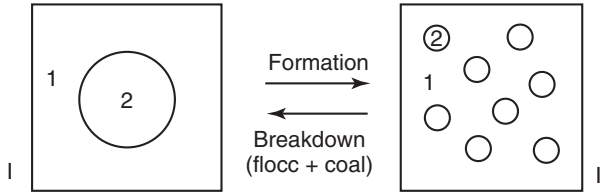


Figure 1.3 Schematic representation of emulsion formation and breakdown.

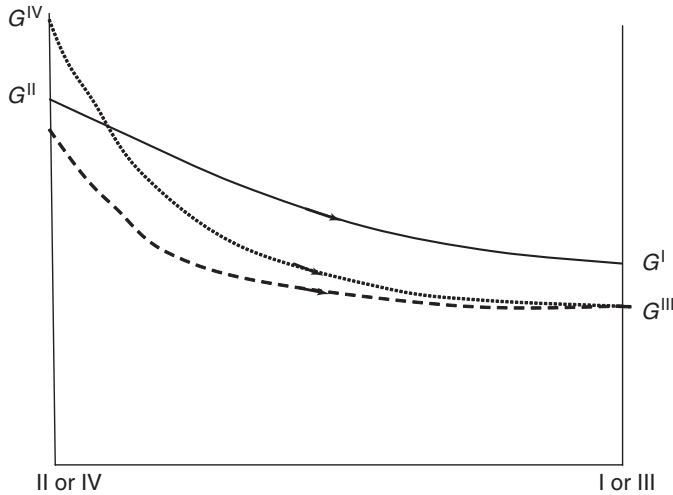


Figure 1.4 Free energy path in emulsion breakdown – (straight line) Floc. + coal.; (dashed line) Floc. + coal. + Sed.; and (dotted line) Floc. + coal. + sed. + Ostwald ripening.

(since producing a large number of droplets is accompanied by an increase in configurational entropy), which is equal to $T\Delta S^{\text{conf}}$.

From the second law of thermodynamics

$$\Delta G^{\text{form}} = \Delta A\gamma_{12} - T\Delta S^{\text{conf}} \quad (1.5)$$

In most cases, $\Delta A\gamma_{12} \gg -T\Delta S^{\text{conf}}$, which means that ΔG^{form} is positive, that is, the formation of emulsions is nonspontaneous and the system is thermodynamically unstable. In the absence of any stabilization mechanism, the emulsion will break by flocculation, coalescence, Ostwald ripening, or combination of all these processes. This is illustrated in Figure 1.4 that shows several paths for emulsion breakdown processes.

In the presence of a stabilizer (surfactant and/or polymer), an energy barrier is created between the droplets, and therefore, the reversal from state II to state I becomes noncontinuous as a result of the presence of these energy barriers. This is illustrated in Figure 1.5. In the presence of the above energy barriers, the system becomes kinetically stable.

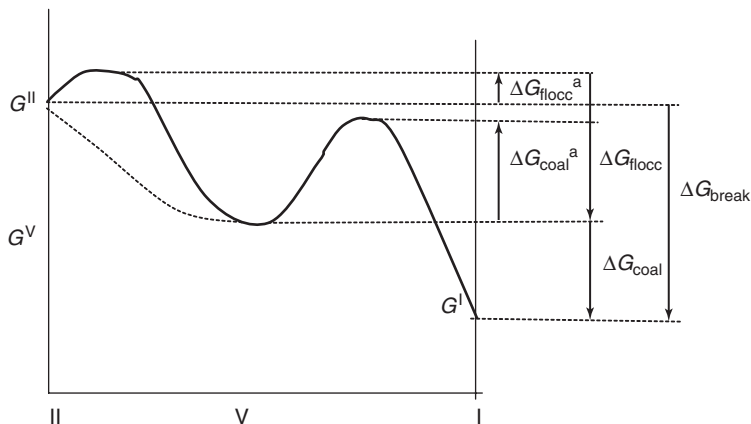


Figure 1.5 Schematic representation of free energy path for breakdown (flocculation and coalescence) for systems containing an energy barrier.

1.5

Interaction Energies (Forces) between Emulsion Droplets and Their Combinations

Generally speaking, there are three main interaction energies (forces) between emulsion droplets and these are discussed in the following sections.

1.5.1

van der Waals Attraction

The van der Waals attraction between atoms or molecules is of three different types: dipole–dipole (Keesom), dipole-induced dipole (Debye), and dispersion (London) interactions. The Keesom and Debye attraction forces are vectors, and although dipole–dipole or dipole-induced dipole attraction is large, they tend to cancel because of the different orientations of the dipoles. Thus, the most important are the London dispersion interactions that arise from charge fluctuations. With atoms or molecules consisting of a nucleus and electrons that are continuously rotating around the nucleus, a temporary dipole is created as a result of charge fluctuations. This temporary dipole induces another dipole in the adjacent atom or molecule. The interaction energy between two atoms or molecules G_a is short range and is inversely proportional to the sixth power of the separation distance r between the atoms or molecules

$$G_a = -\frac{\beta}{r^6} \quad (1.6)$$

where β is the London dispersion constant that is determined by the polarizability of the atom or molecule.

Hamaker [4] suggested that the London dispersion interactions between atoms or molecules in macroscopic bodies (such as emulsion droplets) can be added resulting in strong van der Waals attraction, particularly at close distances of

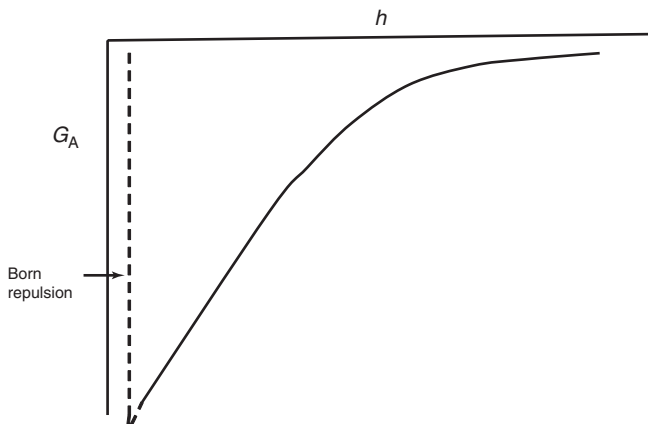


Figure 1.6 Variation of the van der Waals attraction energy with separation distance.

separation between the droplets. For two droplets with equal radii R , at a separation distance h , the van der Waals attraction G_A is given by the following equation (due to Hamaker)

$$G_A = -\frac{AR}{12h} \quad (1.7)$$

where A is the effective Hamaker constant

$$A = \left(A_{11}^{1/2} - A_{22}^{1/2} \right)^2 \quad (1.8)$$

where A_{11} and A_{22} are the Hamaker constants of droplets and dispersion medium, respectively.

The Hamaker constant of any material depends on the number of atoms or molecules per unit volume q and the London dispersion constant β

$$A = \pi^2 q^2 \beta \quad (1.9)$$

G_A increases very rapidly with decrease of h (at close approach). This is illustrated in Figure 1.6 that shows the van der Waals energy–distance curve for two emulsion droplets with separation distance h .

In the absence of any repulsion, flocculation is very fast producing large clusters. To counteract the van der Waals attraction, it is necessary to create a repulsive force. Two main types of repulsion can be distinguished depending on the nature of the emulsifier used: electrostatic (due to the creation of double layers) and steric (due to the presence of adsorbed surfactant or polymer layers).

1.5.2

Electrostatic Repulsion

This can be produced by adsorption of an ionic surfactant as shown in Figure 1.7, which shows a schematic picture of the structure of the double layer according to

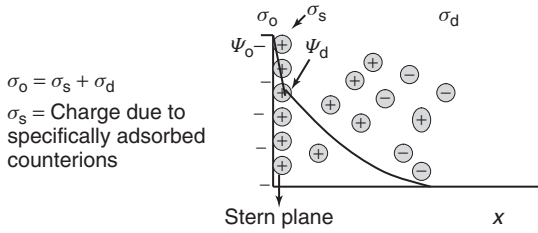


Figure 1.7 Schematic representation of double layers produced by adsorption of an ionic surfactant.

Gouy–Chapman and Stern pictures [3]. The surface potential ψ_o decreases linearly to ψ_d (Stern or zeta potential) and then exponentially with increase of distance x . The double-layer extension depends on electrolyte concentration and valency (the lower the electrolyte concentration and the lower the valency the more extended the double layer is).

When charged colloidal particles in a dispersion approach each other such that the double layer begins to overlap (particle separation becomes less than twice the double-layer extension), repulsion occurs. The individual double layers can no longer develop unrestrictedly because the limited space does not allow complete potential decay [3, 4]. This is illustrated in Figure 1.8 for two flat, which clearly shows that when the separation distance h between the emulsion droplets becomes smaller than twice the double-layer extension, the potential at the midplane between the surfaces is not equal to zero (which would be the case when h is larger than twice the double-layer extension) plates.

The repulsive interaction G_{el} is given by the following expression:

$$G_{el} = 2\pi R\epsilon_r\epsilon_o\psi_o^2 \ln [1 + \exp(-\kappa h)] \quad (1.10)$$

where ϵ_r is the relative permittivity and ϵ_o is the permittivity of free space. κ is the Debye–Hückel parameter; $1/\kappa$ is the extension of the double layer (double-layer thickness) that is given by the expression

$$\left(\frac{1}{\kappa}\right) = \left(\frac{\epsilon_r\epsilon_o kT}{2n_o Z_i^2 e^2}\right) \quad (1.11)$$

where k is the Boltzmann constant, T is the absolute temperature, n_o is the number of ions per unit volume of each type present in bulk solution, Z_i is the valency of the ions, and e is the electronic charge.

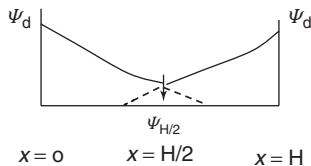


Figure 1.8 Schematic representation of double-layer overlap.

Values of $1/\kappa$ at various 1 : 1 electrolyte concentrations are given below

C (mol dm^{-3})	10^{-5}	10^{-4}	10^{-3}	10^{-2}	10^{-1}
$1/\kappa$ (nm)	100	33	10	3.3	1

The double-layer extension decreases with increase of electrolyte concentration. This means that the repulsion decreases with increase of electrolyte concentration as illustrated in Figure 1.9

$$G_T = G_{el} + G_A \quad (1.12)$$

A schematic representation of the force (energy)–distance curve according to the Derjaguin, Landau, Verwey, and Overbeek (DLVO) theory is given in Figure 1.10.

The above presentation is for a system at low electrolyte concentration. At large h , attraction prevails resulting in a shallow minimum (G_{sec}) of the order of few kilotesla units. At very short h , $V_A \gg G_{el}$, resulting in a deep primary minimum (several hundred kilotesla units). At intermediate h , $G_{el} > G_A$, resulting in a maximum (energy barrier) whose height depends on ψ_0 (or ζ) and electrolyte concentration and valency – the energy maximum is usually kept >25 kT units.

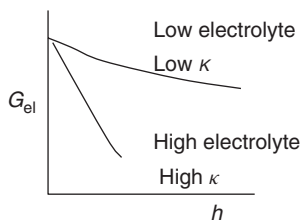


Figure 1.9 Variation of G_{el} with h at low and high electrolyte concentrations.

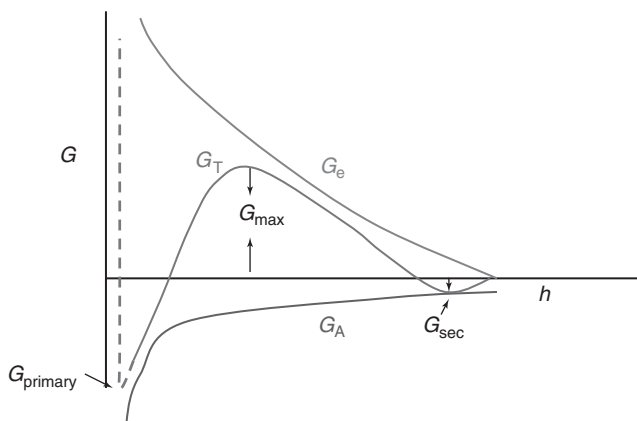


Figure 1.10 Total energy–distance curve according to the DLVO theory.

The energy maximum prevents close approach of the droplets, and flocculation into the primary minimum is prevented. The higher the value of ψ_0 and the lower the electrolyte concentration and valency, the higher the energy maximum. At intermediate electrolyte concentrations, weak flocculation into the secondary minimum may occur.

Combination of van der Waals attraction and double-layer repulsion results in the well-known theory of colloid stability due to DLVO theory [5, 6].

1.5.3

Steric Repulsion

This is produced by using nonionic surfactants or polymers, for example, alcohol ethoxylates, or A-B-A block copolymers PEO-PPO-PEO (where PEO refers to polyethylene oxide and PPO refers to polypropylene oxide), as illustrated in Figure 1.11.

The “thick” hydrophilic chains (PEO in water) produce repulsion as a result of two main effects [7]:

- 1) Unfavorable mixing of the PEO chains, when these are in good solvent conditions (moderate electrolyte and low temperatures). This is referred to as the *osmotic or mixing free energy of interaction* that is given by the expression

$$\frac{G_{\text{mix}}}{kT} = \left(\frac{4\pi}{V_1} \right) \phi_2^2 N_{\text{av}} \left(\frac{1}{2} - \chi \right) \left(\delta - \frac{h}{2} \right)^2 \left(3R + 2\delta + \frac{h}{2} \right) \quad (1.13)$$

V_1 is the molar volume of the solvent, ϕ_2 is the volume fraction of the polymer chain with a thickness δ , and χ is the Flory–Huggins interaction parameter.

When $\chi < 0.5$, G_{mix} is positive and the interaction is repulsive. When $\chi > 0.5$, G_{mix} is negative and the interaction is attractive. When $\chi = 0.5$, $G_{\text{mix}} = 0$ and this is referred to as the θ -condition.

- 2) Entropic, volume restriction, or elastic interaction, G_{el} .

This results from the loss in configurational entropy of the chains on significant overlap. Entropy loss is unfavorable and, therefore, G_{el} is always positive.

Combination of G_{mix} , G_{el} with G_A gives the total energy of interaction G_T (theory of steric stabilization)

$$G_T = G_{\text{mix}} + G_{\text{el}} + G_A \quad (1.14)$$

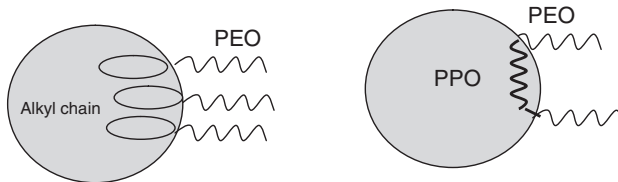


Figure 1.11 Schematic representation of adsorbed layers.

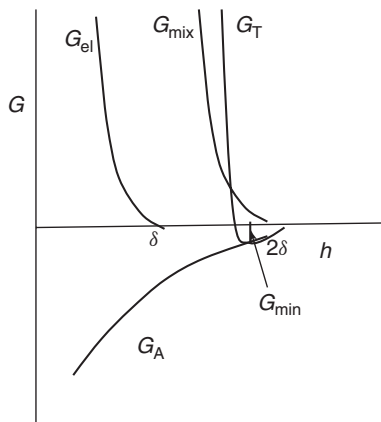


Figure 1.12 Schematic representation of the energy–distance curve for a sterically stabilized emulsion.

A schematic representation of the variation of G_{mix} , G_{el} , and G_A with h is given in Figure 1.12. G_{mix} increases very sharply with decrease of h when the latter becomes less than 2δ . G_{el} increases very sharply with decrease of h when the latter becomes smaller than δ . G_T increases very sharply with decrease of h when the latter becomes less than 2δ .

Figure 1.12 shows that there is only one minimum (G_{min}) whose depth depends on R , δ , and A . At a given droplet size and Hamaker constant, the larger the adsorbed layer thickness, the smaller the depth of the minimum. If G_{min} is made sufficiently small (large δ and small R), one may approach thermodynamic stability. This is illustrated in Figure 1.13 that shows the energy–distance curves as a function of δ/R . The larger the value of δ/R , the smaller the value of G_{min} . In this case, the system may approach thermodynamic stability as is the case with nanodispersions.

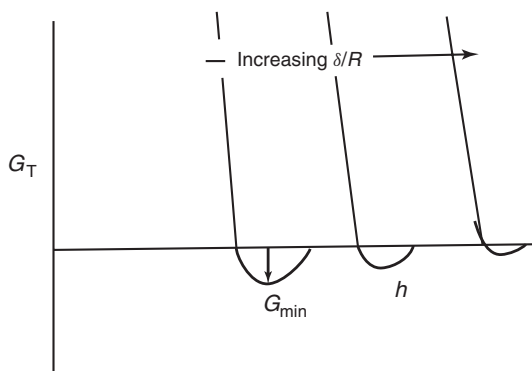


Figure 1.13 Variation of G_T with h at various δ/R values.

1.6

Adsorption of Surfactants at the Liquid/Liquid Interface

Surfactants accumulate at interfaces, a process described as adsorption. The simplest interfaces are the air/water (A/W) and O/W. The surfactant molecule orients itself at the interface with the hydrophobic portion orienting toward the hydrophobic phase (air or oil) and the hydrophilic portion orienting at the hydrophilic phase (water). This is schematically illustrated in Figure 1.14. As a result of adsorption, the surface tension of water is reduced from its value of 72 mN m^{-1} before adsorption to $\sim 30\text{--}40 \text{ mN m}^{-1}$ and the interfacial tension for the O/W system decreases from its value of 50 mN m^{-1} (for an alkane oil) before adsorption to a value of $1\text{--}10 \text{ mN m}^{-1}$ depending on the nature of the surfactant.

Two approaches can be applied to treat surfactant adsorption at the A/L and L/L interface [3]: Gibbs approach treats the process as an equilibrium phenomenon. In this case, one can apply the second law of thermodynamics. Equation of state approach whereby the surfactant film is treated as a “two-dimensional” layer with a surface pressure π . The Gibbs approach allows one to obtain the surfactant adsorption from surface tension measurements. The equation of state approach allows one to study the surfactant orientation at the interface. In this section, only the Gibbs approach is described.

1.6.1

The Gibbs Adsorption Isotherm

Gibbs derived a thermodynamic relationship between the variation of surface or interfacial tension with concentration and the amount of surfactant adsorbed Γ (moles per unit area), referred to as the *surface excess*. At equilibrium, the Gibbs free energy $dG^\sigma = 0$ and the Gibbs–Deuhem equation becomes

$$dG^\sigma = -S^\sigma dT + Ad\gamma + \sum n_i^\sigma d\mu_i = 0 \quad (1.15)$$

At constant temperature

$$Ad\gamma = - \sum n_i^\sigma d\mu_i \quad (1.16)$$

or

$$d\gamma = - \sum \frac{n_i^\sigma}{A} d\mu_i = - \sum \Gamma_i^\sigma d\mu_i \quad (1.17)$$

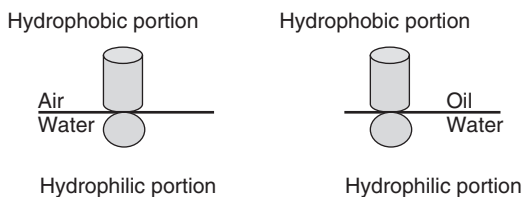


Figure 1.14 Schematic representation of orientation of surfactant molecules.

For a surfactant (component 2) adsorbed at the surface of a solvent (component 1)

$$-d\gamma = \Gamma_1^\sigma d\mu_1 + \Gamma_2^\sigma d\mu_2 \quad (1.18)$$

If the Gibbs dividing surface is used and the assumption $\Gamma_1^\sigma = 0$ is made

$$-d\gamma = \Gamma_{2,1}^\sigma d\mu_2 \quad (1.19)$$

The chemical potential of the surfactant μ_2 is given by the expression

$$\mu_2 = \mu_2^0 + RT \ln a_2^L \quad (1.20)$$

where μ_2^0 is the standard chemical potential and a_2^L is the activity of surfactant that is equal to $C_2 f_2 \sim x_2 f_2$ where C_2 is the concentration in moles per cubic decimeter and x_2 is the mole fraction that is equal to $C_2 / (C_2 + 55.5)$ for a dilute solution, and f_2 is the activity coefficient that is also ~ 1 in dilute solutions.

Differentiating Eq. (1.20), one obtains

$$d\mu_2 = RT d \ln a_2^L \quad (1.21)$$

Combining Eqs. (1.19) and (1.21),

$$-d\gamma = \Gamma_{2,1}^\sigma RT d \ln a_2^L \quad (1.22)$$

or

$$\frac{d\gamma}{d \ln a_2^L} = -RT \Gamma_{2,1}^L \quad (1.23)$$

In dilute solutions, $f_2 \sim 1$ and

$$\frac{d\gamma}{d \ln C_2} = -\Gamma_2 RT \quad (1.24)$$

Equations (1.23) and (1.24) are referred to as the *Gibbs adsorption equations*, which show that Γ_2 can be determined from the experimental results of variation of γ with $\log C_2$ as illustrated in Figure 1.15 for the A/W and O/W interfaces.

Γ_2 can be calculated from the linear portion of the γ - $\log C$ curve just before the critical micelle concentration (cmc)

$$\text{Slope} = -\frac{d\gamma}{d \log C_2} = -2.303 \Gamma_2 RT \quad (1.25)$$

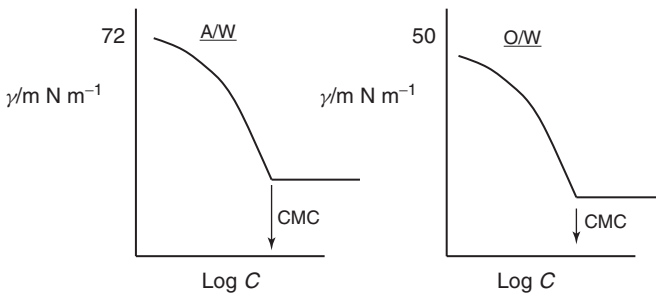


Figure 1.15 Surface or interfacial tension – $\log C$ curves.

From Γ_2 , the area per molecule of surfactant (or ion) can be calculated

$$\text{Area/molecule} = \frac{1}{\Gamma_2 N_{\text{av}}} (\text{m}^2) = \frac{10^{18}}{\Gamma_2 N_{\text{av}}} (\text{nm}^2) \quad (1.26)$$

N_{av} is Avogadro's constant that is equal to 6.023×10^{23} .

The area per surfactant ion or molecule gives information on the orientation of the ion or molecule at the interface. The area depends on whether the molecules lie flat or vertical at the interface. It also depends on the length of the alkyl chain length (if the molecules lie flat) or the cross-sectional area of the head group (if the molecules lie vertical. For example, for an ionic surfactant such as SDS, the area per molecule depends on the orientation. If the molecule lies flat, the area is determined by the area occupied by the alkyl chain and that by the sulfate head group. In this case, the area per molecule increases with increase in the alkyl chain length and will be in the range of 1–2 nm². In contrast, for vertical orientation, the area per molecule is determined by the cross-sectional area of the sulfate group, which is ~ 0.4 nm² and virtually independent of the alkyl chain length. Addition of electrolytes screens the charge on the head group and hence the area per molecule decreases. For nonionic surfactants such as alcohol ethoxylates, the area per molecule for flat orientation is determined by the length of the alkyl chain and the number of ethylene oxide (EO) units. For vertical orientation, the area per molecule is determined by the cross-sectional area of the PEO chain and this increases with increase in the number of EO units.

At concentrations just before the break point, the slope of the γ -log C curve is constant

$$\left(\frac{\partial \gamma}{\partial \log C_2} \right) = \text{constant} \quad (1.27)$$

This indicates that saturation of the interface occurs just below the cmc.

Above the break point ($C > \text{cmc}$), the slope is 0,

$$\left(\frac{\partial \gamma}{\partial \log C_2} \right) = 0 \quad (1.28)$$

or

$$\gamma = \text{constant} \times \log C_2 \quad (1.29)$$

As γ remains constant above the cmc, then C_2 or a_2 of the monomer must remain constant.

Addition of surfactant molecules above the cmc must result in association to form micelles that have low activity, and hence, a_2 remains virtually constant.

The hydrophilic head group of the surfactant molecule can also affect its adsorption. These head groups can be unionized, for example, alcohol or PEO; weakly ionized, for example, COOH; or strongly ionized, for example, sulfates $-\text{O}-\text{SO}_3^-$, sulfonates $-\text{SO}_3^-$, or ammonium salts $-\text{N}^+(\text{CH}_3)_3$. The adsorption of the different surfactants at the A/W and O/W interface depends on the nature of the head group. With nonionic surfactants, repulsion between the head groups is smaller than with ionic head groups and adsorption occurs from dilute solutions; the

cmc is low, typically 10^{-5} to 10^{-4} mol dm $^{-3}$. Nonionic surfactants with medium PEO form closely packed layers at $C < \text{cmc}$. Adsorption is slightly affected by moderate addition of electrolytes or change in the pH. Nonionic surfactant adsorption is relatively simple and can be described by the Gibbs adsorption equation.

With ionic surfactants, adsorption is more complicated depending on the repulsion between the head groups and addition of indifferent electrolyte. The Gibbs adsorption equation has to be solved to take into account the adsorption of the counterions and any indifferent electrolyte ions.

For a strong surfactant electrolyte such as $R - O - SO_3^- Na^+ (R^- Na^+)$

$$\Gamma_2 = -\frac{1}{2RT} \left(\frac{\partial \gamma}{\partial \ln a_{\pm}} \right) \quad (1.30)$$

The factor 2 in Eq. (1.30) arises because both surfactant ion and counterion must be adsorbed to maintain neutrality. $(\partial \gamma / \partial \ln a_{\pm})$ is twice as large for an unionized surfactant molecule.

For a nonadsorbed electrolyte such as NaCl, any increase in $Na^+ \cdot R^-$ concentration produces a negligible increase in Na^+ concentration ($d\mu_{Na^+}^+$ is negligible – $d\mu_{Cl^-}$ is also negligible).

$$\Gamma_2 = -\frac{1}{RT} \left(\frac{\partial \gamma}{\partial \ln C_{NaR}} \right) \quad (1.31)$$

which is identical to the case of nonionics.

The above analysis shows that many ionic surfactants may behave like nonionics in the presence of a large concentration of an indifferent electrolyte such as NaCl.

1.6.2

Mechanism of Emulsification

As mentioned before, to prepare an emulsions oil, water, surfactant, and energy are needed. This can be considered from a consideration of the energy required to expand the interface, $\Delta A\gamma$ (where ΔA is the increase in interfacial area when the bulk oil with area A_1 produces a large number of droplets with area A_2 ; $A_2 \gg A_1$, γ is the interfacial tension). As γ is positive, the energy to expand the interface is large and positive; this energy term cannot be compensated by the small entropy of dispersion $T\Delta S$ (which is also positive) and the total free energy of formation of an emulsion, ΔG given by Eq. (1.5) is positive. Thus, emulsion formation is nonspontaneous and energy is required to produce the droplets.

The formation of large droplets (few micrometers) as is the case for macroemulsions is fairly easy, and hence, high-speed stirrers such as the Ultraturrax or Silverson Mixer are sufficient to produce the emulsion. In contrast, the formation of small drops (submicrometer as is the case with nanoemulsions) is difficult and this requires a large amount of surfactant and/or energy. The high energy required for the formation of nanoemulsions can be understood from a consideration of the Laplace pressure Δp (the difference in pressure between inside and outside the droplet) as given by Eqs. (1.3) and (1.4).

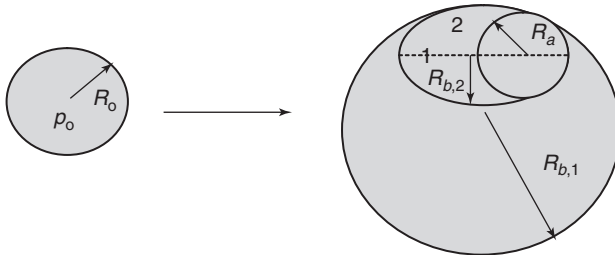


Figure 1.16 Illustration of increase in Laplace pressure when a spherical drop is deformed to a prolate ellipsoid.

To break up a drop into smaller ones, it must be strongly deformed and this deformation increases Δp . This is illustrated in Figure 1.16 that shows the situation when a spherical drop deforms into a prolate ellipsoid [8].

Near 1, there is only one radius of curvature R_a , whereas near 2, there are two radii of curvature $R_{b,1}$ and $R_{b,2}$. Consequently, the stress needed to deform the drop is higher for a smaller drop – as the stress is generally transmitted by the surrounding liquid via agitation, higher stresses need more vigorous agitation, and hence more energy is needed to produce smaller drops.

Surfactants play major roles in the formation of emulsions: by lowering the interfacial tension, p is reduced and hence the stress needed to break up a drop is reduced. Surfactants also prevent coalescence of newly formed drops.

Figure 1.17 shows an illustration of the various processes occurring during emulsification, break up of droplets, adsorption of surfactants, and droplet collision (which may or may not lead to coalescence) [8].

Each of the above processes occurs numerous times during emulsification and the timescale of each process is very short, typically a microsecond. This shows

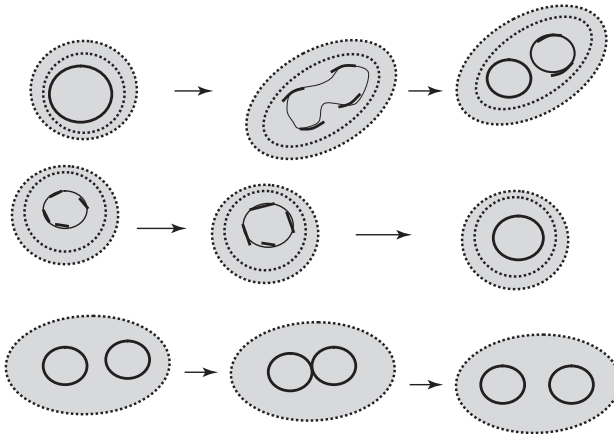


Figure 1.17 Schematic representation of the various processes occurring during emulsion formation. The drops are depicted by thin lines and the surfactant by heavy lines and dots.

that the emulsification process is a dynamic process and events that occur in a microsecond range could be very important.

To describe emulsion formation, one has to consider two main factors: hydrodynamics and interfacial science. In hydrodynamics, one has to consider the type of flow: laminar flow and turbulent flow. This depends on the Reynolds number as is discussed later.

To assess emulsion formation, one usually measures the droplet size distribution using, for example, laser diffraction techniques. A useful average diameter d is

$$d_{nm} = \left(\frac{S_m}{S_n} \right)^{1/(n-m)} \quad (1.32)$$

In most cases, d_{32} (the volume/surface average or Sauter mean) is used. The width of the size distribution can be given as the variation coefficient c_m , which is the standard deviation of the distribution weighted with d^m divided by the corresponding average d . Generally, C_2 is used that corresponds to d_{32} .

An alternative way to describe the emulsion quality is to use the specific surface area A (surface area of all emulsion droplets per unit volume of emulsion)

$$A = \pi s^2 = \frac{6\varphi}{d_{32}} \quad (1.33)$$

1.6.3

Methods of Emulsification

Several procedures may be applied for emulsion preparation, and these range from simple pipe flow (low agitation energy L); static mixers and general stirrers (low to medium energy, L–M); high-speed mixers such as the Ultraturrex (M); colloid mills and high-pressure homogenizers (high energy, H); and ultrasound generators (M–H). The method of preparation can be continuous (C) or batch-wise (B): pipe flow and static mixers – C; stirrers and Ultraturrex – B,C; colloid mill and high-pressure homogenizers – C; and ultrasound – B,C.

In all methods, there is liquid flow; unbounded and strongly confined flow. In the unbounded flow, any droplets are surrounded by a large amount of flowing liquid (the confining walls of the apparatus are far away from most of the droplets). The forces can be frictional (mostly viscous) or inertial. Viscous forces cause shear stresses to act on the interface between the droplets and the continuous phase (primarily in the direction of the interface). The shear stresses can be generated by laminar flow (LV) or turbulent flow (TV); this depends on the Reynolds number Re

$$Re = \frac{vl\rho}{\eta} \quad (1.34)$$

where v is the linear liquid velocity, ρ is the liquid density, and η is its viscosity. l is a characteristic length that is given by the diameter of flow through a cylindrical tube and by twice the slit width in a narrow slit.

For laminar flow, $Re \gtrsim 1000$, whereas for turbulent flow, $Re \gtrsim 2000$. Thus, whether the regime is linear or turbulent depends on the scale of the apparatus, the flow rate, and the liquid viscosity [9–12].

If the turbulent eddies are much larger than the droplets, they exert shear stresses on the droplets. If the turbulent eddies are much smaller than the droplets, inertial forces will cause disruption.

In bounded flow, other relations hold. If the smallest dimension of the part of the apparatus in which the droplets are disrupted (say a slit) is comparable to droplet size, other relations hold (the flow is always laminar). A different regime prevails if the droplets are directly injected through a narrow capillary into the continuous phase (injection regime), that is, membrane emulsification.

Within each regime, an essential variable is the intensity of the forces acting; the viscous stress during laminar flow σ_{viscous} is given by

$$\sigma_{\text{viscous}} = \eta G \quad (1.35)$$

where G is the velocity gradient.

The intensity in turbulent flow is expressed by the power density ε (the amount of energy dissipated per unit volume per unit time); for laminar flow,

$$\varepsilon = \eta G^2 \quad (1.36)$$

The most important regimes are laminar/viscous (LV), turbulent/viscous (TV), and turbulent/inertial (TI). For water as the continuous phase, the regime is always TI. For higher viscosity of the continuous phase ($\eta_C = 0.1$ Pa s), the regime is TV. For still higher viscosity or a small apparatus (small l), the regime is LV. For very small apparatus (as is the case with most laboratory homogenizers), the regime is nearly always LV.

For the above regimes, a semiquantitative theory is available that can give the timescale and magnitude of the local stress σ_{ext} , the droplet diameter d , timescale of droplets deformation τ_{def} , timescale of surfactant adsorption τ_{ads} , and mutual collision of droplets.

An important parameter that describes droplet deformation is the Weber number We (which gives the ratio of the external stress over the Laplace pressure)

$$We = \frac{G \eta_C R}{2\gamma} \quad (1.37)$$

The viscosity of the oil plays an important role in the breakup of droplets; the higher the viscosity, the longer it will take to deform a drop. The deformation time τ_{def} is given by the ratio of oil viscosity to the external stress acting on the drop

$$\tau_{\text{def}} = \frac{\eta_D}{\sigma_{\text{ext}}} \quad (1.38)$$

The viscosity of the continuous phase η_C plays an important role in some regimes: for TI regime, η_C has no effect on droplet size. For turbulent viscous regime, larger η_C leads to smaller droplets. For laminar viscous, the effect is even stronger.

1.6.4

Role of Surfactants in Emulsion Formation

Surfactants lower the interfacial tension γ , and this causes a reduction in droplet size. The latter decrease with decrease in γ . For laminar flow, the droplet diameter is proportional to γ ; for TI regime, the droplet diameter is proportional to $\gamma^{3/5}$.

The effect of reducing γ on the droplet size is illustrated in Figure 1.18, which shows a plot of the droplet surface area A and mean drop size d_{32} as a function of surfactant concentration m for various systems.

The amount of surfactant required to produce the smallest drop size will depend on its activity a (concentration) in the bulk that determines the reduction in γ , as given by the Gibbs adsorption equation

$$-d\gamma = RT\Gamma d \ln a \quad (1.39)$$

where R is the gas constant, T is the absolute temperature, and Γ is the surface excess (number of moles adsorbed per unit area of the interface).

Γ increases with increase in surfactant concentration and eventually it reaches a plateau value (saturation adsorption). This is illustrated in Figure 1.19 for various emulsifiers.

The value of γ obtained depends on the nature of the oil and surfactant used; small molecules such as nonionic surfactants lower γ more than polymeric surfactants such as PVA.

Another important role of the surfactant is its effect on the interfacial dilational modulus ε

$$\varepsilon = \frac{d\gamma}{d \ln A} \quad (1.40)$$

During emulsification, an increase in the interfacial area A takes place and this causes a reduction in Γ . The equilibrium is restored by adsorption of surfactant from the bulk, but this takes time (shorter times occur at higher surfactant activity).

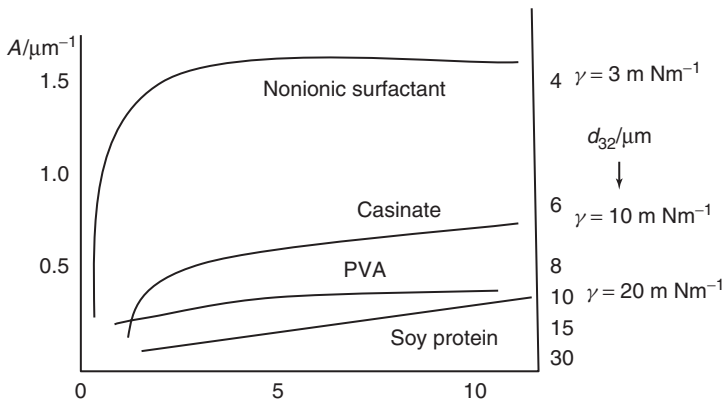


Figure 1.18 Variation of A and d_{32} with m for various surfactant systems.

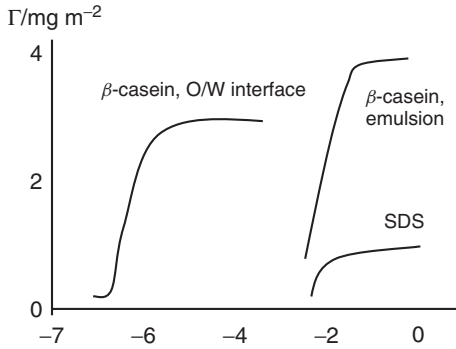


Figure 1.19 Variation of Γ (mg m^{-2}) with $\log C_{\text{eq}}/\text{wt}\%$ – the oils are β -casein (O–W interface) toluene, β -casein (emulsions) soybean, and SDS benzene.

Thus, ε is small at small a and also at large a . Because of the lack or slowness of equilibrium with polymeric surfactants, ε will not be the same for expansion and compression of the interface.

In practice, surfactant mixtures are used and these have pronounced effects on γ and ε . Some specific surfactant mixtures give lower γ values than either of the two individual components. The presence of more than one surfactant molecule at the interface tends to increase ε at high surfactant concentrations. The various components vary in surface activity. Those with the lowest γ tend to predominate at the interface, but if present at low concentrations, it may take long time before reaching the lowest value. Polymer–surfactant mixtures may show some synergetic surface activity.

1.6.5

Role of Surfactants in Droplet Deformation

Apart from their effect on reducing γ , surfactants play major roles in deformation and breakup of droplets – this is summarized as follows. Surfactants allow the existence of interfacial tension gradients, which is crucial for the formation of stable droplets. In the absence of surfactants (clean interface), the interface cannot withstand a tangential stress; the liquid motion will be continuous (Figure 1.20a).

If a liquid flows along the interface with surfactants, the latter will be swept downstream causing an interfacial tension gradient (Figure 1.20b). A balance of forces will be established

$$\eta \left[\frac{dV_x}{dy} \right]_{y=0} = -\frac{dy}{dx} \quad (1.41)$$

If the γ -gradient can become large enough, it will arrest the interface. If the surfactant is applied at one site of the interface, a γ -gradient is formed that will cause the interface to move roughly at a velocity given by

$$v = 1.2 [\eta \rho z]^{-1/3} |\Delta\gamma|^{2/3} \quad (1.42)$$

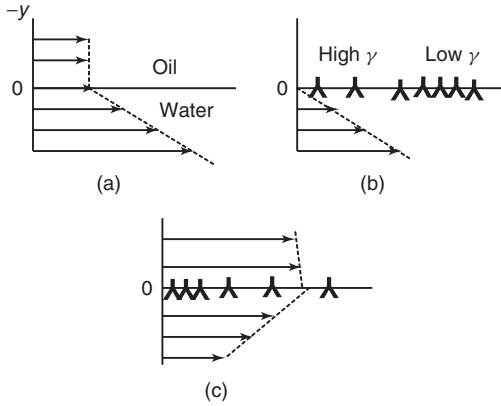


Figure 1.20 Interfacial tension gradients and flow near an oil/water interface: (a) no surfactant; (b) velocity gradient causes an interfacial tension gradient; and (c) interfacial tension gradient causes flow (Marangoni effect).

The interface will then drag some of the bordering liquid with it (Figure 1.20c).

Interfacial tension gradients are very important in stabilizing the thin liquid film between the droplets, which is very important during the beginning of emulsification (films of the continuous phase may be drawn through the disperse phase and collision is very large). The magnitude of the γ -gradients and the Marangoni effect depends on the surface dilational modulus ε , which for a plane interface with one surfactant-containing phase, is given by the expression

$$\varepsilon = \frac{-d\gamma/d \ln \Gamma}{(1 + 2\xi + 2\xi^2)^{1/2}} \quad (1.43)$$

$$\xi = \frac{dm_C}{d\Gamma} \left(\frac{D}{2\omega} \right)^{1/2} \quad (1.44)$$

$$\omega = \frac{d \ln A}{dt} \quad (1.45)$$

where D is the diffusion coefficient of the surfactant and ω represents a timescale (time needed for doubling the surface area) that is roughly equal to τ_{def} .

During emulsification, ε is dominated by the magnitude of the denominator in Eq. (1.43) because ξ remains small. The value of $dm_C/d\Gamma$ tends to go to very high values when Γ reaches its plateau value; ε goes to a maximum when m_C is increased.

For conditions that prevail during emulsification, ε increases with m_C and it is given by the relationship

$$\varepsilon = \frac{d\pi}{d \ln \Gamma} \quad (1.46)$$

where π is the surface pressure ($\pi = \gamma_o - \gamma$). Figure 1.21 shows the variation of π with $\ln \Gamma$; ε is given by the slope of the line.

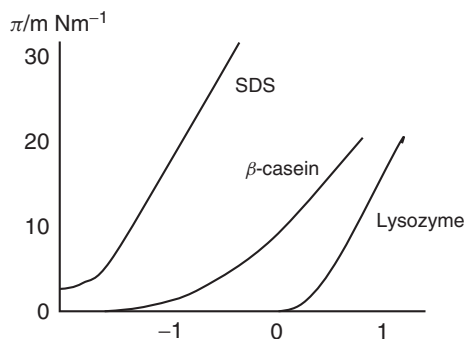


Figure 1.21 π versus $\ln \Gamma$ for various emulsifiers.

The SDS shows a much higher ε value when compared with β -casein and lysozyme – this is because the value of Γ is higher for SDS. The two proteins show difference in their ε values, which may be attributed to the conformational change that occurs on adsorption.

The presence of a surfactant means that during emulsification the interfacial tension needs not to be the same everywhere (Figure 1.20). This has two consequences: (i) the equilibrium shape of the drop is affected and (ii) any γ -gradient formed will slow down the motion of the liquid inside the drop (this diminishes the amount of energy needed to deform and break up the drop).

Another important role of the emulsifier is to prevent coalescence during emulsification. This is certainly not due to the strong repulsion between the droplets, because the pressure at which two drops are pressed together is much greater than the repulsive stresses. The counteracting stress must be due to the formation of γ -gradients. When two drops are pushed together, liquid will flow out from the thin layer between them, and the flow will induce a γ -gradient. This was shown in Figure 1.20c. This produces a counteracting stress given by

$$\tau_{\Delta\gamma} \approx \frac{2 |\Delta\gamma|}{(1/2)d} \quad (1.47)$$

The factor 2 follows from the fact that two interfaces are involved. Taking a value of $\Delta\gamma = 10 \text{ mN m}^{-1}$, the stress amounts to 40 kPa (which is of the same order of magnitude as the external stress).

Closely related to the above mechanism is the Gibbs-Marangoni effect [13–17], schematically represented in Figure 1.22. The depletion of surfactant in the thin film between approaching drops results in γ -gradient without liquid flow being involved. This results in an inward flow of liquid that tends to drive the drops apart.

The Gibbs–Marangoni effect also explains the Bancroft rule, which states that the phase in which the surfactant is most soluble forms the continuous phase. If the surfactant is in the droplets, a γ -gradient cannot develop and the drops would

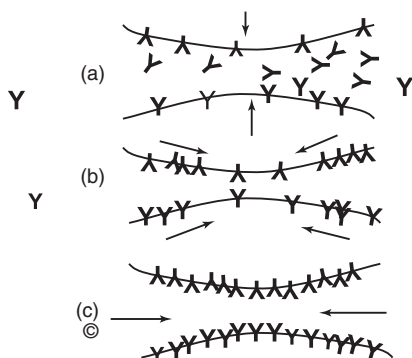


Figure 1.22 Schematic representation of the Gibbs–Marangoni effect for two approaching drops.

be prone to coalescence. Thus, surfactants with $HLB > 7$ (hydrophilic–lipophilic balance) tend to form O/W emulsions and $HLB < 7$ tend to form W/O emulsions.

The Gibbs–Marangoni effect also explains the difference between surfactants and polymers for emulsification – polymers give larger drops when compared with surfactants. Polymers give a smaller value of ε at small concentrations when compared to surfactants (Figure 1.21).

Various other factors should also be considered for emulsification: The disperse phase volume fraction ϕ . An increase in ϕ leads to increase in droplet collision and hence coalescence during emulsification. With increase in ϕ , the viscosity of the emulsion increases and could change the flow from being turbulent to being laminar (LV regime).

The presence of many particles results in a local increase in velocity gradients. This means that G increases. In turbulent flow, increase in ϕ will induce turbulence depression. This results in larger droplets. Turbulence depression by added polymers tends to remove the small eddies, resulting in the formation of larger droplets.

If the mass ratio of surfactant to continuous phase is kept constant, increase in ϕ results in decrease in surfactant concentration and hence an increase in γ_{eq} resulting in larger droplets. If the mass ratio of surfactant to disperse phase is kept constant, the above changes are reversed.

General conclusions cannot be drawn because several of the above-mentioned mechanism may come into play. Experiments using a high-pressure homogenizer at various ϕ values at constant initial m_C (regime TI changing to TV at higher ϕ) showed that with increasing ϕ (>0.1) the resulting droplet diameter increased and the dependence on energy consumption became weaker. Figure 1.23 shows a comparison of the average droplet diameter versus power consumption using different emulsifying machines. It can be seen that the smallest droplet diameters were obtained when using the high-pressure homogenizers.

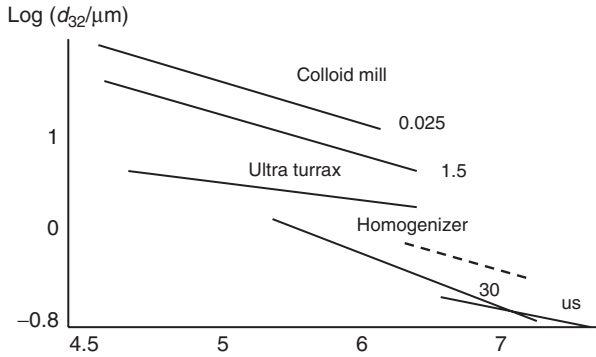


Figure 1.23 Average droplet diameters obtained in various emulsifying machines as a function of energy consumption p – the number near the curves denotes the viscosity ratio λ – the results for the homogenizer are for $\phi = 0.04$ (solid line) and $\phi = 0.3$ (broken line) – us means ultrasonic generator.

1.7

Selection of Emulsifiers

1.7.1

The Hydrophilic–Lipophilic Balance (HLB) Concept

The selection of different surfactants in the preparation of either O/W or W/O emulsions is often still made on an empirical basis. A semiempirical scale for selecting surfactants is the HLB number developed by Griffin [18]. This scale is based on the relative percentage of hydrophilic to lipophilic (hydrophobic) groups in the surfactant molecule(s). For an O/W emulsion droplet, the hydrophobic chain resides in the oil phase, whereas the hydrophilic head group resides in the aqueous phase. For a W/O emulsion droplet, the hydrophilic group(s) reside in the water droplet, whereas the lipophilic groups reside in the hydrocarbon phase.

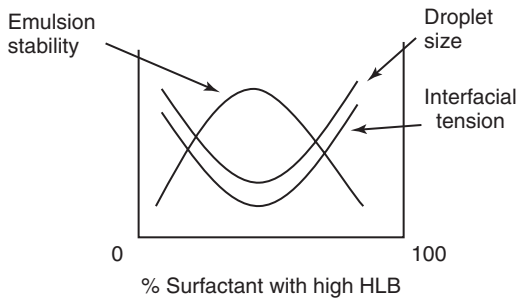
Table 1.2 gives a guide to the selection of surfactants for a particular application. The HLB number depends on the nature of the oil. As an illustration, Table 1.3 gives the required HLB numbers to emulsify various oils.

Table 1.2 Summary of HLB ranges and their applications.

HLB range	Application
3–6	W/O emulsifier
7–9	Wetting agent
8–18	O/W emulsifier
13–15	Detergent
15–18	Solubilizer

Table 1.3 Required HLB numbers to emulsify various oils.

Oil	W/O emulsion	O/W emulsion
Paraffin oil	4	10
Beeswax	5	9
Linolin, anhydrous	8	12
Cyclohexane	—	15
Toluene	—	15

**Figure 1.24** Variation of emulsion stability, droplet size, and interfacial tension with percentage surfactant with high HLB number.

The relative importance of the hydrophilic and lipophilic groups was first recognized when using mixtures of surfactants containing varying proportions of a low and high HLB number.

The efficiency of any combination (as judged by phase separation) was found to pass a maximum when the blend contained a particular proportion of the surfactant with the higher HLB number. This is illustrated in Figure 1.24 that shows the variation of emulsion stability, droplet size, and interfacial tension with percentage surfactant with high HLB number.

The average HLB number may be calculated from additivity

$$\text{HLB} = x_1\text{HLB}_1 + x_2\text{HLB}_2 \quad (1.48)$$

where x_1 and x_2 are the weigh fractions of the two surfactants with HLB_1 and HLB_2 .

Griffin developed simple equations for calculation of the HLB number of relatively simple nonionic surfactants. For a polyhydroxy fatty acid ester

$$\text{HLB} = 20 \left(1 - \frac{S}{A} \right) \quad (1.49)$$

S is the saponification number of the ester and A is the acid number. For a glyceryl monostearate, $S = 161$ and $A = 198$; the HLB is 3.8 (suitable for W/O emulsion).

For a simple alcohol ethoxylate, the HLB number can be calculated from the weight percentage of ethylene oxide (E) and polyhydric alcohol (P)

$$\text{HLB} = \frac{E + P}{5} \quad (1.50)$$

If the surfactant contains PEO as the only hydrophilic group, the contribution from one OH group neglected

$$\text{HLB} = \frac{E}{5} \quad (1.51)$$

For a nonionic surfactant $\text{C}_{12}\text{H}_{25}-\text{O}-(\text{CH}_2-\text{CH}_2-\text{O})_6$, the HLB is 12 (suitable for O/W emulsion).

The above simple equations cannot be used for surfactants containing propylene oxide or butylene oxide. They cannot be also applied for ionic surfactants. Davies [19, 20] devised a method for calculating the HLB number for surfactants from their chemical formulae, using empirically determined group numbers. A group number is assigned to various component groups. A summary of the group numbers for some surfactants is given in Table 1.4.

The HLB is given by the following empirical equation:

$$\text{HLB} = 7 + \sum(\text{hydrophilic group Nos}) - \sum(\text{lipohilic group Nos}) \quad (1.52)$$

Davies has shown that the agreement between HLB numbers calculated from the above equation and those determined experimentally is quite satisfactory.

Various other procedures were developed to obtain a rough estimate of the HLB number. Griffin found good correlation between the cloud point of 5% solution of various ethoxylated surfactants and their HLB number.

Davies [17, 18] attempted to relate the HLB values to the selective coalescence rates of emulsions. Such correlations were not realized since it was found that the emulsion stability and even its type depends to a large extent on the method of

Table 1.4 HLB group numbers.

Hydrophilic	Group number
$-\text{SO}_4\text{Na}^+$	38.7
$-\text{COO}$	21.2
$-\text{COONa}$	19.1
N(tertiary amine)	9.4
Ester (sorbitan ring)	6.8
$-\text{O}-$	1.3
$\text{CH}-$ (sorbitan ring)	0.5
Lipophilic ($-\text{CH}-$), ($-\text{CH}_2-$), CH_3	0.475
Derived	
$-\text{CH}_2 - \text{CH}_2 - \text{O}$	0.33
$-\text{CH}_2 - \text{CH}_2 - \text{CH}_2 - \text{O}-$	-0.15

dispersing the oil into the water and vice versa. At best, the HLB number can only be used as a guide for selecting optimum compositions of emulsifying agents.

One may take any pair of emulsifying agents, which fall at opposite ends of the HLB scale, for example, Tween 80 (sorbitan monooleate with 20 mol EO, HLB = 15) and Span 80 (sorbitan monooleate, HLB = 5) using them in various proportions to cover a wide range of HLB numbers. The emulsions should be prepared in the same way, with a small percentage of the emulsifying blend. The stability of the emulsions is then assessed at each HLB number from the rate of coalescence or qualitatively by measuring the rate of oil separation. In this way, one may be able to find the optimum HLB number for a given oil. Having found the most effective HLB value, various other surfactant pairs are compared at this HLB value to find the most effective pair.

1.7.2

The Phase Inversion Temperature (PIT) Concept

Shinoda and coworkers [21, 22] found that many O/W emulsions stabilized with nonionic surfactants undergo a process of inversion at a critical temperature (phase inversion temperature, PIT). The PIT can be determined by following the emulsion conductivity (small amount of electrolyte is added to increase the sensitivity) as a function of temperature. The conductivity of the O/W emulsion increases with increase of temperature till the PIT is reached, above which there will be a rapid reduction in conductivity (W/O emulsion is formed). Shinoda and coworkers found that the PIT is influenced by the HLB number of the surfactant. The size of the emulsion droplets was found to depend on the temperature and HLB number of the emulsifiers. The droplets are less stable toward coalescence close to the PIT. However, by rapid cooling of the emulsion, a stable system may be produced. Relatively stable O/W emulsions were obtained when the PIT of the system was 20–65 °C higher than the storage temperature. Emulsions prepared at a temperature just below the PIT followed by rapid cooling generally have smaller droplet sizes. This can be understood if one considers the change of interfacial tension with temperature as is illustrated in Figure 1.25. The interfacial tension decreases with increase of temperature reaching a minimum close to the PIT, after which it increases.

Thus, the droplets prepared close to the PIT are smaller than those prepared at lower temperatures. These droplets are relatively unstable toward coalescence near the PIT, but by rapid cooling of the emulsion, one can retain the smaller size. This procedure may be applied to prepare mini (nano) emulsions.

The optimum stability of the emulsion was found to be relatively insensitive to changes in the HLB value or the PIT of the emulsifier, but instability was very sensitive to the PIT of the system.

It is essential, therefore, to measure the PIT of the emulsion as a whole (with all other ingredients).

At a given HLB value, stability of the emulsions against coalescence increases markedly as the molar mass of both the hydrophilic and lipophilic components

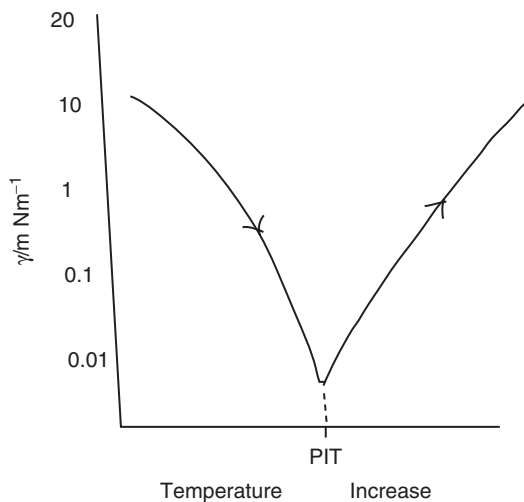


Figure 1.25 Variation of interfacial tension with temperature increase for an O/W emulsion.

increases. The enhanced stability using high-molecular-weight surfactants (polymeric surfactants) can be understood from a consideration of the steric repulsion that produces more stable films. Films produced using macromolecular surfactants resist thinning and disruption thus reducing the possibility of coalescence. The emulsions showed maximum stability when the distribution of the PEO chains was broad. The cloud point is lower but the PIT is higher than in the corresponding case for narrow size distributions. The PIT and HLB number are directly related parameters.

Addition of electrolytes reduces the PIT and hence an emulsifier with a higher PIT value is required when preparing emulsions in the presence of electrolytes. Electrolytes cause dehydration of the PEO chains and in effect this reduces the cloud point of the nonionic surfactant. One needs to compensate for this effect by using a surfactant with higher HLB. The optimum PIT of the emulsifier is fixed if the storage temperature is fixed.

In view of the above correlation between PIT and HLB and the possible dependence of the kinetics of droplet coalescence on the HLB number, Sherman and coworkers suggested the use of PIT measurements as a rapid method for assessing emulsion stability. However, one should be careful in using such methods for assessment of the long-term stability because the correlations were based on a very limited number of surfactants and oils.

Measurement of the PIT can at best be used as a guide for the preparation of stable emulsions. Assessment of the stability should be evaluated by following the droplet size distribution as a function of time using a Coulter counter or light diffraction techniques. Following the rheology of the emulsion as a function of time and temperature may also be used for assessment of the stability against coalescence. Care should be taken in analyzing the rheological results. Coalescence

results in an increase in the droplet size and this is usually followed by a reduction in the viscosity of the emulsion. This trend is only observed if the coalescence is not accompanied by flocculation of the emulsion droplets (which results in an increase in the viscosity). Ostwald ripening can also complicate the analysis of the rheological data.

1.7.3

The Cohesive Energy Ratio (CER) Concept

Beerbower and Hills [23] considered the dispersing tendency on the oil and water interfaces of the surfactant or emulsifier in terms of the ratio of the cohesive energies of the mixtures of oil with the lipophilic portion of the surfactant and the water with the hydrophilic portion. They used the Winsor R_o concept, which is the ratio of the intermolecular attraction of oil molecules (O) and lipophilic portion of surfactant (L), C_{LO} , to that of water (W) and hydrophilic portion (H), C_{HW}

$$R_o = \frac{C_{LO}}{C_{HW}} \quad (1.53)$$

Several interaction parameters may be identified at the oil and water sides of the interface. One can identify at least nine interaction parameters as schematically represented in Figure 1.26.

In the absence of emulsifier, there will be only three interaction parameters: C_{OO} , C_{WW} , C_{OW} ; if $C_{OW} \ll C_{WW}$, the emulsion breaks.

The above interaction parameters may be related to the Hildebrand solubility parameter [24] δ (at the oil side of the interface) and the Hansen [25] nonpolar, hydrogen bonding, and polar contributions to δ at the water side of the interface. The solubility parameter of any component is related to its heat of vaporization ΔH by the expression

$$\delta^2 = \frac{\Delta H - RT}{V_m} \quad (1.54)$$

where V_m is the molar volume.

Hansen considered δ (at the water side of the interface) to consist of three main contributions, a dispersion contribution, δ_d ; a polar contribution, δ_p ; and a

- C_{LL} , C_{OO} , C_{LO} (at oil side)
- C_{HH} , C_{WW} , C_{HW} (at water side)
- C_{LW} , C_{HO} , C_{LH} (at the interface)

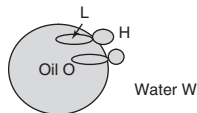


Figure 1.26 The cohesive energy ratio concept.

hydrogen-bonding contribution, δ_h . These contributions have different weighting factors

$$\delta^2 = \delta_d^2 + 0.25\delta_p^2 + \delta_h^2 \quad (1.55)$$

Beerbower and Hills used the following expression for the HLB number

$$\text{HLB} = 20 \left(\frac{M_H}{M_L + M_H} \right) = 20 \left(\frac{V_H \rho_H}{V_L \rho_L + V_H \rho_H} \right) \quad (1.56)$$

where M_H and M_L are the molecular weights of the hydrophilic and lipophilic portions of the surfactants, respectively. V_L and V_H are their corresponding molar volumes whereas ρ_H and ρ_L are the densities, respectively.

The cohesive energy ratio (CER) was originally defined by Winsor, Eq. (1.53).

When $C_{LO} > C_{HW}$, $R > 1$ and a W/O emulsion forms. If $C_{LO} < C_{HW}$, $R < 1$ and an O/W emulsion forms. If $C_{LO} = C_{HW}$, $R = 1$ and a planer system results – this denotes the inversion point.

R_o can be related to V_L , δ_L and V_H , δ_H by the expression

$$R_o = \frac{V_L \delta_L^2}{V_H \delta_H^2} \quad (1.57)$$

Using Eq. (1.55)

$$R_o = \frac{V_L (\delta_d^2 + 0.25\delta_p^2 + 0.25\delta_h^2)_L}{V_H (\delta_d^2 + 0.25\delta_p^2 + 0.25\delta_h^2)_H} \quad (1.58)$$

Combining Eqs. (1.57) and (1.58), one obtains the following general expression for the CER

$$R_o = \left(\frac{20}{\text{HLB}} - 1 \right) \frac{\rho_H (\delta_d^2 + 0.25\delta_p^2 + 0.25\delta_h^2)_L}{\rho_L (\delta_d^2 + 0.25\delta_p^2 + 0.25\delta_h^2)_H} \quad (1.59)$$

For O/W systems, $\text{HLB} = 12-15$ and $R_o = 0.58-0.29$ ($R_o < 1$). For W/O systems, $\text{HLB} = 5-6$ and $R_o = 2.3-1.9$ ($R_o > 1$). For a planer system, $\text{HLB} = 8-10$ and $R_o = 1.25-0.85$ ($R_o \sim 1$)

The R_o equation combines both the HLB and cohesive energy densities – it gives a more quantitative estimate of emulsifier selection. R_o considers HLB, molar volume, and chemical match. The success of this approach depends on the availability of data on the solubility parameters of the various surfactant portions. Some values are tabulated in the book by Barton [26].

1.7.4

The Critical Packing Parameter (CPP) for Emulsion Selection

The critical packing parameter (CPP) is a geometric expression relating the hydrocarbon chain volume (v) and length (l) and the interfacial area occupied by the head group (a) [27]

$$\text{CPP} = \frac{v}{l_c a_o} \quad (1.60)$$

a_o is the optimal surface area per head group and l_c is the critical chain length.

Regardless of the shape of any aggregated structure (spherical or cylindrical micelle or a bilayer), no point within the structure can be farther from the hydrocarbon-water surface than l_c . The critical chain length, l_c , is roughly equal but less than the fully extended length of the alkyl chain.

The above concept can be applied to predict the shape of an aggregated structure. Consider a spherical micelle with radius r and aggregation number n ; the volume of the micelle is given by

$$\left(\frac{4}{3}\right) \pi r^3 = nv \quad (1.61)$$

where v is the volume of a surfactant molecule.

The area of the micelle is given by

$$4\pi r^2 = na_o \quad (1.62)$$

where a_o is the area per surfactant head group.

Combining Eqs. (1.61) and (1.62)

$$a_o = \frac{3v}{r} \quad (1.63)$$

The cross-sectional area of the hydrocarbon chain a is given by the ratio of its volume to its extended length l_c

$$a = \frac{v}{l_c} \quad (1.64)$$

From Eqs. (1.63) and (1.64)

$$\text{CPP} = \frac{a}{a_o} = \left(\frac{1}{3}\right) \left(\frac{r}{l_c}\right) \quad (1.65)$$

As $r < l_c$, then $\text{CPP} \leq (1/3)$.

For a cylindrical micelle with length d and radius r

$$\text{Volume of the micelle} = \pi r^2 d = nv \quad (1.66)$$

$$\text{Area of the micelle} = 2\pi rd = na_o \quad (1.67)$$

Combining Eqs. (1.66) and (1.67)

$$a_o = \frac{2v}{r} \quad (1.68)$$

$$a = \frac{v}{l_c} \quad (1.69)$$

$$\text{CPP} = \frac{a}{a_o} = \left(\frac{1}{2}\right) \left(\frac{r}{l_c}\right) \quad (1.70)$$

As $r < l_c$, then $(1/3) < \text{CPP} \leq (1/2)$.

For vesicles (liposomes), $1 > \text{CPP} \geq (2/3)$ and for lamellar micelles $P \sim 1$. For inverse micelles, $\text{CPP} > 1$. A summary of the various shapes of micelles and their CPP is given in Table 1.5.

Table 1.5 Critical packing parameter and various shapes of micelles.

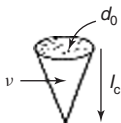









Lipid	Critical packing parameter $vianlc$	Critical packing shape	Structures formed
Single-chained lipids (surfactants) with large head group areas: SDS in low salt	$<1/3$	Cone 	Spherical micelles 
Single-chained lipids with small head group areas: SDS and CTAB in high salt Nonionic lipids	$1/3-1/2$	Truncated cone 	Cylindrical micelles 
Double-chained lipids with large head group areas, fluid chains: Phosphatidyl choline (lecithin) Phosphatidyl serine Phosphatidyl glycerol Phosphatidyl inositol Phosphatidic acid Sphingomyelin, DGDG ^a Dihexadecyl phosphate Dialkyl dimethyl ammonium Salts	$1/2-1$	Truncated cone 	Flexible bilayers, vesicles 
Double-chained lipids with small head group areas, anionic lipids in high salt, saturated frozen chains: Phosphatidyl ethanolamine Phosphatidyl serine + Ca ²¹	~ 1	Cylinder 	Planar bilayers 

Table 1.5 (continued)

Lipid	Critical packing parameter vianlc	Critical packing shape	Structures formed
Double-chained lipids with small head group areas, nonionic lipids, poly(cis) unsaturated chains, high T: Unsaturated, phosphatidyl ethanolamine Cardiolipin} + Ca ²⁺ Phosphatidic acid + Ca ²⁺ Cholesterol, MGDG ^b	>1	Inverted truncated cone or wedge 	Inverted micelles 

^aDGDG, digalactosyl diglyceride, diglucosyldiglyceride;

^bMGDG, monogalactosyl diglyceride, monoglucosyl diglyceride.

Surfactants that make spherical micelles with the above packing constraints, that is, $CPP \leq (1/3)$, are more suitable for O/W emulsions. Surfactants with $CPP > 1$, that is, forming inverted micelles, are suitable for the formation of W/O emulsions.

1.8

Creaming or Sedimentation of Emulsions

This is the result of gravity, when the density of the droplets and the medium are not equal. When the density of the disperse phase is lower than that of the medium, creaming occurs, whereas if the density of the disperse phase is higher than that of the medium, sedimentation occurs. Figure 1.27 gives a schematic picture for creaming of emulsions for three cases [28].

Case (a) represents the situation for small droplets ($< 0.1 \mu\text{m}$, i.e., nanoemulsions) whereby the Brownian diffusion kT (where k is the Boltzmann constant and T is the absolute temperature) exceeds the force of gravity (mass \times acceleration due to gravity g)

$$kT \gg \frac{4}{3}\pi R^3 \Delta\rho gL \quad (1.71)$$

where R is the droplet radius, $\Delta\rho$ is the density difference between the droplets and the medium, and L is the height of the container.

Case (b) represents emulsions consisting of “monodisperse” droplets with radius $> 1 \mu\text{m}$. In this case, the emulsion separates into two distinct layers with the droplets forming a cream or sediment leaving the clear supernatant liquid. This situation is seldom observed in practice. Case (c) is that for a polydisperse

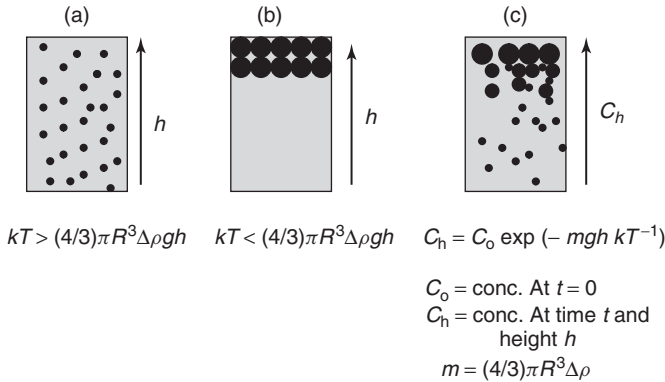


Figure 1.27 (a–c) Representation of creaming of emulsions.

(practical) emulsions, in which case the droplets will cream or sediment at various rates. In the last case, a concentration gradient build up with the larger droplets staying at the top of the cream layer or the bottom of the sediment

$$C(h) = C_0 \exp\left(-\frac{mgh}{kT}\right) \quad (1.72)$$

$C(h)$ is the concentration (or volume fraction ϕ) of droplets at height h , whereas C_0 is the concentration at the top or bottom of the container.

1.8.1

Creaming or Sedimentation Rates

- 1) Very dilute emulsions ($\phi < 0.01$). In this case, the rate could be calculated using Stokes' law that balances the hydrodynamic force with gravity force

$$\text{Hydrodynamic force} = 6\pi\eta_0 R v_0 \quad (1.73)$$

$$\text{Gravity force} = \frac{4}{3}\pi R^3 \Delta \rho g \quad (1.74)$$

$$v_0 = \frac{2}{9} \frac{\Delta \rho g R^2}{\eta_0} \quad (1.75)$$

v_0 is the Stokes' velocity and η_0 is the viscosity of the medium.

For an O/W emulsion with $\Delta \rho = 0.2$ in water ($\eta_0 \sim 10^{-3}$ Pa-s), the rate of creaming or sedimentation is $\sim 4.4 \times 10^{-5} \text{ m s}^{-1}$ for $10 \mu\text{m}$ droplets and $\sim 4.4 \times 10^{-7} \text{ m s}^{-1}$ for $1 \mu\text{m}$ droplets. This means that in a 0.1 m container creaming or sedimentation of the $10 \mu\text{m}$ droplets is complete in $\sim 0.6 \text{ h}$ and for the $1 \mu\text{m}$ droplets this takes $\sim 60 \text{ h}$.

- 2) Moderately concentrated emulsions ($0.2 < \phi < 0.1$). In this case, one has to take into account the hydrodynamic interaction between the droplets, which

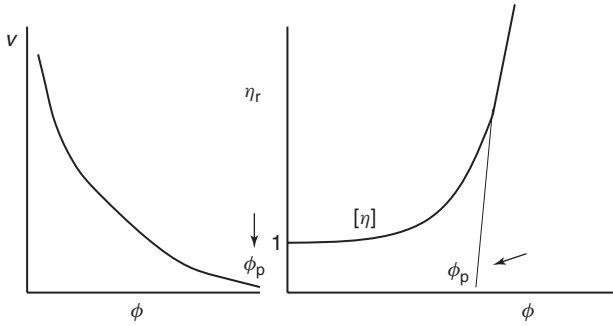


Figure 1.28 Variation of v and η_r with ϕ .

reduces the Stokes velocity to a value v given by the following expression [29]

$$v = v_0(1 - k\phi) \quad (1.76)$$

where k is a constant that accounts for hydrodynamic interaction. k is of the order of 6.5, which means that the rate of creaming or sedimentation is reduced by about 65%.

- 3) Concentrated emulsions ($\phi > 0.2$). The rate of creaming or sedimentation becomes a complex function of ϕ as is illustrated in Figure 1.28, which also shows the change of relative viscosity η_r with ϕ .

As can be seen from the above figure, v decreases with increase in ϕ and ultimately it approaches zero when ϕ exceeds a critical value, ϕ_p , which is the so-called “maximum packing fraction.” The value of ϕ_p for monodisperse “hard spheres” ranges from 0.64 (for random packing) to 0.74 for hexagonal packing. The value of ϕ_p exceeds 0.74 for polydisperse systems. Also for emulsions that are deformable, ϕ_p can be much larger than 0.74.

The above figure also shows that when ϕ approaches ϕ_p , η_r approaches ∞ . In practice, most emulsions are prepared at ϕ values well below ϕ_p , usually in the range 0.2–0.5, and under these conditions, creaming or sedimentation is the rule rather than the exception. Several procedures may be applied to reduce or eliminate creaming or sedimentation, and these are discussed in the following sections.

1.8.2

Prevention of Creaming or Sedimentation

- 1) **Matching density of oil and aqueous phases:** Clearly, if $\Delta\rho = 0$, $v = 0$; However, this method is seldom practical. Density matching, if possible, only occurs at one temperature.
- 2) **Reduction of droplet size:** As the gravity force is proportional to R^3 , then if R is reduced by a factor of 10, the gravity force is reduced by 1000. Below a certain droplet size (which also depends on the density difference between oil and water), the Brownian diffusion may exceed gravity and creaming or sedimentation is prevented. This is the principle of formulation of nanoemulsions

(with size range 20–200 nm), which may show very little or no creaming or sedimentation. The same applies for microemulsions (size range 5–50 nm)

- 3) **Use of “thickeners”:** These are high-molecular-weight polymers, natural, or synthetic such as Xanthan gum, hydroxyethyl cellulose, alginates, and carragenans. To understand the role of these “thickeners,” let us consider the gravitational stresses exerted during creaming or sedimentation

$$\text{Stress} = \text{mass of drop} \times \text{acceleration of gravity} = \frac{4}{3}\pi R^3 \Delta\rho g \quad (1.77)$$

To overcome such stress, one needs a restoring force

$$\text{Restoring force} = \text{area of drop} \times \text{stress of rop} = 4\pi R^2 \sigma_p \quad (1.78)$$

Thus, the stress exerted by the droplet σ_p is given by

$$\sigma_p = \frac{\Delta\rho Rg}{3} \quad (1.79)$$

Simple calculation shows that σ_p is in the range 10^{-3} to 10^{-1} Pa, which implies that for prediction of creaming or sedimentation one needs to measure the viscosity at such low stresses. This can be obtained by using constant stress or creep measurements.

The above-described “thickeners” satisfy the criteria for obtaining very high viscosities at low stresses or shear rates. This can be illustrated from plots of shear stress σ and viscosity η versus shear rate $\dot{\gamma}$ (or shear stress), as shown in Figure 1.29. These systems are described as “pseudoplastic” or shear thinning. The low shear (residual or zero shear rate) viscosity $\eta(o)$ can reach several thousand Pascal-second, and such high values prevent creaming or sedimentation [30, 31].

The above behavior is obtained above a critical polymer concentration (C^*), which can be located from plots of $\log \eta$ versus $\log C$ as shown in Figure 1.30. Below C^* , the $\log \eta - \log C$ curve has a slope in the region of 1, whereas above C^* , the slope of the line exceeds 3. In most cases, good correlation between the rate of creaming or sedimentation and $\eta(o)$ is obtained.

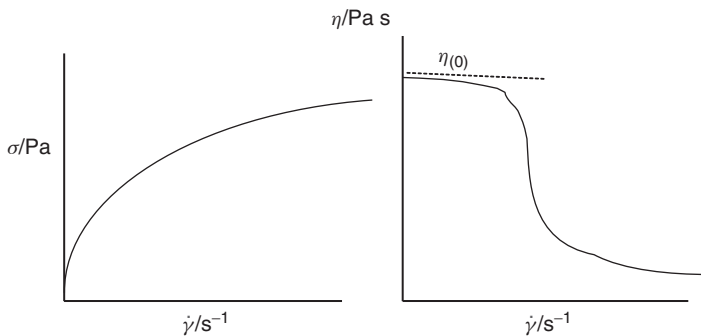


Figure 1.29 Variation of stress σ and viscosity η with shear rate $\dot{\gamma}$.

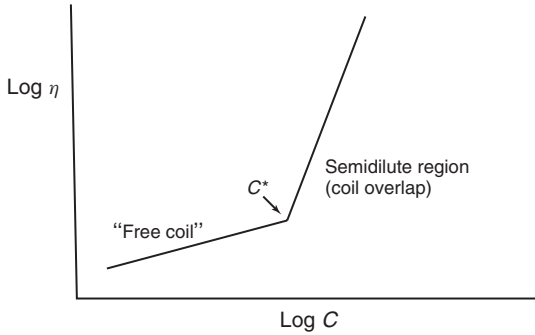


Figure 1.30 Variation of $\log \eta$ with $\log C$ for polymer solutions.

- 4) **Controlled flocculation:** As discussed earlier, the total energy distance of separation curve for electrostatically stabilized shows a shallow minimum (secondary minimum) at relatively long distance of separation between the droplets. By addition of small amounts of electrolyte, such minimum can be made sufficiently deep for weak flocculation to occur. The same applied for sterically stabilized emulsions, which show only one minimum, whose depth can be controlled by reducing the thickness of the adsorbed layer. This can be obtained by reducing the molecular weight of the stabilizer and/or addition of a nonsolvent for the chains (e.g., electrolyte).

The above phenomenon of weak flocculation may be applied to reduce creaming or sedimentation, although in practice this is not easy since one has also to control the droplet size.

- 5) **Depletion flocculation:** This is obtained by addition of “free” (nonadsorbing) polymer in the continuous phase [32]. At a critical concentration, or volume fraction of free polymer, ϕ_p^+ , weak flocculation occurs because the free polymer coils become “squeezed out” from between the droplets. This is illustrated in Figure 1.31 that shows the situation when the polymer volume fraction exceeds the critical concentration.

The osmotic pressure outside the droplets is higher than in between the droplets, and this results in attraction whose magnitude depends on the concentration of the free polymer and its molecular weight, as well as the droplet size and ϕ . The value of ϕ_p^+ decreases with increase in the molecular weight of the free polymer. It also decreases as the volume fraction of the emulsion increases.

The above weak flocculation can be applied to reduce creaming or sedimentation although it suffers from the following drawbacks: (i) temperature dependence; as the temperature increases, the hydrodynamic radius of the free polymer decreases (due to dehydration) and hence more polymer will be required to achieve the same effect at lower temperatures. (ii) If the free polymer concentration is increased above a certain limit, phase separation may occur and the flocculated emulsion droplets may cream or sediment faster than in the absence of the free polymer.

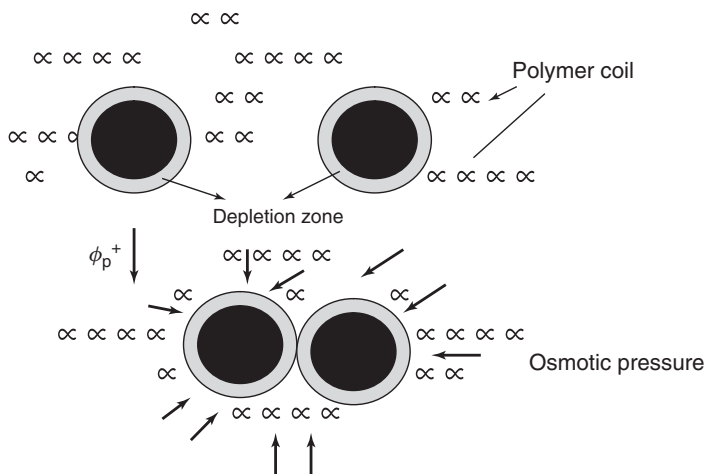


Figure 1.31 Schematic representation of depletion flocculation.

1.9

Flocculation of Emulsions

Flocculation is the result of van der Waals attraction that is universal for all disperse systems. The van der Waals attraction G_A was described before. As shown in Figure 1.6, G_A is inversely proportional to the droplet–droplet distance of separation h and it depends on the effective Hamaker constant A of the emulsion system. One way to overcome the van der Waals attraction is by electrostatic stabilization using ionic surfactants, which results in the formation of electrical double layers that introduce a repulsive energy that overcomes the attractive energy. Emulsions stabilized by electrostatic repulsion become flocculated at intermediate electrolyte concentrations (see below). The second and most effective method of overcoming flocculation is by “steric stabilization” using nonionic surfactants or polymers. Stability may be maintained in electrolyte solutions (as high as 1 mol dm^{-3} depending on the nature of the electrolyte) and up to high temperatures (in excess of 50°C) provided that the stabilizing chains (e.g., PEO) are still in better than θ -conditions ($\chi < 0.5$).

1.9.1

Mechanism of Emulsion Flocculation

This can occur if the energy barrier is small or absent (for electrostatically stabilized emulsions) or when the stabilizing chains reach poor solvency (for sterically stabilized emulsions, i.e., $\chi > 0.5$). For convenience, flocculation of electrostatically and sterically stabilized emulsions are discussed separately.

1.9.1.1 Flocculation of Electrostatically Stabilized Emulsions

As discussed before, the condition for kinetic stability is $G_{\max} > 25 kT$. When $G_{\max} < 5 kT$, flocculation occurs. Two types of flocculation kinetics may be distinguished: fast flocculation with no energy barrier and slow flocculation when an energy barrier exists.

The fast flocculation kinetics was treated by Smoluchowki [33], who considered the process to be represented by second-order kinetics and the process is simply diffusion controlled. The number of particles n at any time t may be related to the final number (at $t = 0$) n_o by the following expression

$$n = \frac{n_o}{1 + kn_o t} \quad (1.80)$$

where k is the rate constant for fast flocculation that is related to the diffusion coefficient of the particles D , that is

$$k = 8\pi DR \quad (1.81)$$

D is given by the Stokes–Einstein equation

$$D = \frac{kT}{6\pi\eta R} \quad (1.82)$$

Combining Eqs. (1.81) and (1.82)

$$k = \frac{4 kT}{3 \eta} = 5.5 \times 10^{-18} \text{ m}^3 \text{ s}^{-1} \text{ for water at } 25^\circ \text{C} \quad (1.83)$$

The half life $t_{1/2}$ ($n = (1/2)n_o$) can be calculated at various n_o or volume fraction ϕ as given in Table 1.6.

The slow flocculation kinetics was treated by Fuchs [34] who related the rate constant k to the Smoluchowski rate by the stability constant W

$$W = \frac{k_o}{k} \quad (1.84)$$

W is related to G_{\max} by the following expression [35]

$$W = \frac{1}{2} \exp\left(\frac{G_{\max}}{kT}\right) \quad (1.85)$$

Table 1.6 Half-life of emulsion flocculation.

R (μm)	ϕ			
	10^{-5}	10^{-2}	10^{-1}	5×10^{-1}
0.1	765 s	76 ms	7.6 ms	1.5 ms
1.0	21 h	76 s	7.6 s	1.5 s
10.0	4 mo	21 h	2 h	25 mo

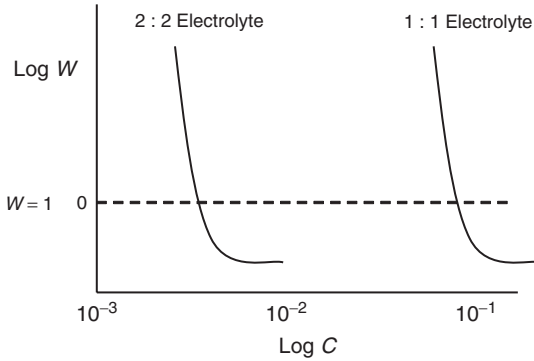


Figure 1.32 Log W –log C curves for electrostatically stabilized emulsions.

As G_{\max} is determined by the salt concentration C and valency, one can derive an expression relating W to C and Z

$$\log W = -2.06 \times 10^9 \left(\frac{R\gamma^2}{Z^2} \right) \log C \quad (1.86)$$

where γ is a function that is determined by the surface potential ψ_o

$$\gamma = \left[\frac{\exp(Ze\psi_o/kT) - 1}{\exp(ZE\psi_o/kT) + 1} \right] \quad (1.87)$$

Plots of log W versus log C are shown in Figure 1.32. The condition log $W = 0$ ($W = 1$) is the onset of fast flocculation. The electrolyte concentration at this point defines the critical flocculation concentration (CFC). Above the CFC, $W < 1$ (due to the contribution of van der Waals attraction that accelerates the rate above the Smoluchowski value). Below the CFC, $W > 1$ and it increases with decrease of electrolyte concentration. The figure also shows that the CFC decreases with increase of valency in accordance to the Scultze–Hardy rule.

Another mechanism of flocculation is that involving the secondary minimum (G_{\min}), which is few kilotesla units. In this case, flocculation is weak and reversible and hence one must consider both the rate of flocculation (forward rate k_f) and deflocculation (backward rate k_b). The rate of decrease of particle number with time is given by the expression

$$-\frac{dn}{dt} = -k_f n^2 + k_b n \quad (1.88)$$

The backward reaction (breakup of weak flocs) reduces the overall rate of flocculation.

1.9.1.2 Flocculation of Sterically Stabilized Emulsions

This occurs when the solvency of the medium for the chain becomes worse than a θ -solvent ($\chi > 0.5$). Under these conditions, G_{mix} becomes negative, that is, attractive and a deep minimum is produced resulting in catastrophic flocculation (referred to as *incipient flocculation*). This is schematically represented in Figure 1.33.

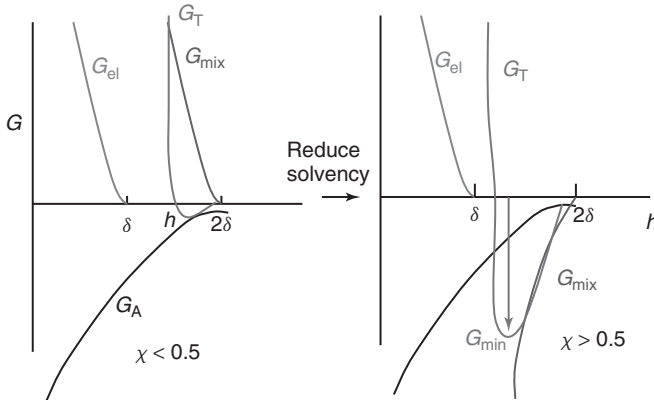


Figure 1.33 Schematic representation of flocculation of sterically stabilized emulsions.

With many systems, good correlation between the flocculation point and the θ -point is obtained.

For example, the emulsion will flocculate at a temperature (referred to as the critical flocculation temperature, CFT) that is equal to the θ -temperature of the stabilizing chain. The emulsion may flocculate at a critical volume fraction of a nonsolvent critical volume fraction (CFV), which is equal to the volume of nonsolvent that brings it to a θ -solvent.

1.9.2

General Rules for Reducing (Eliminating) Flocculation

- 1) **Charge-stabilized emulsions, for example, using ionic surfactants:** The most important criterion is to make G_{\max} as high as possible; this is achieved by three main conditions: high surface or zeta potential, low electrolyte concentration, and low valency of ions.
- 2) **Sterically stabilized emulsions:** Four main criteria are necessary: (i) complete coverage of the droplets by the stabilizing chains. (ii) Firm attachment (strong anchoring) of the chains to the droplets. This requires the chains to be insoluble in the medium and soluble in the oil. However, this is incompatible with stabilization that requires a chain that is soluble in the medium and strongly solvated by its molecules. These conflicting requirements are solved by the use of A-B, A-B-A block, or BA_n graft copolymers (B is the “anchor” chain and A is the stabilizing chain(s)).

Examples of the B chains for O/W emulsions are polystyrene, polymethylmethacrylate, PPO, and alkyl PPO. For the A chain(s), PEO and polyvinyl alcohol are good examples. For W/O emulsions, PEO can form the B chain, whereas the A chain(s) could be polyhydroxy stearic acid (PHS), which is strongly solvated by most oils. (iii) Thick adsorbed layers: the adsorbed layer thickness should be in the range of 5–10 nm. This means that the molecular weight of the stabilizing chains

could be in the range of 1000–5000. (iv) The stabilizing chain should be maintained in good solvent conditions ($\chi < 0.5$) under all conditions of temperature changes on storage.

1.10 Ostwald Ripening

The driving force for Ostwald ripening is the difference in solubility between the small and large droplets (the smaller droplets have higher Laplace pressure and higher solubility than the larger ones). This is illustrated in Figure 1.34 where r_1 decreases and r_2 increases as a result of diffusion of molecules from the smaller to the larger droplets.

The difference in chemical potential between different sized droplets was given by Lord Kelvin [36]

$$S(r) = S(\infty) \exp\left(\frac{2\gamma V_m}{rRT}\right) \quad (1.89)$$

where $S(r)$ is the solubility surrounding a particle of radius r , $S(\infty)$ is the bulk solubility, V_m is the molar volume of the dispersed phase, R is the gas constant, and T is the absolute temperature. The quantity $(2\gamma V_m/RT)$ is termed the *characteristic length*. It has an order of ~ 1 nm or less, indicating that the difference in solubility of a $1 \mu\text{m}$ droplet is on the order of 0.1% or less. Theoretically, Ostwald ripening should lead to condensation of all droplets into a single drop. This does not occur in practice since the rate of growth decreases with increase of droplet size.

For two droplets with radii r_1 and r_2 ($r_1 < r_2$)

$$\frac{RT}{V_m} \ln \left[\frac{S(r_1)}{S(r_2)} \right] = 2\gamma \left[\frac{1}{r_1} - \frac{1}{r_2} \right] \quad (1.90)$$

Equation (1.88) shows that the larger the difference between r_1 and r_2 , the higher the rate of Ostwald ripening.

Ostwald ripening can be quantitatively assessed from plots of the cube of the radius versus time t [37, 38]

$$r^3 = \frac{8}{9} \left[\frac{S(\infty)\gamma V_m D}{\rho RT} \right] t \quad (1.91)$$

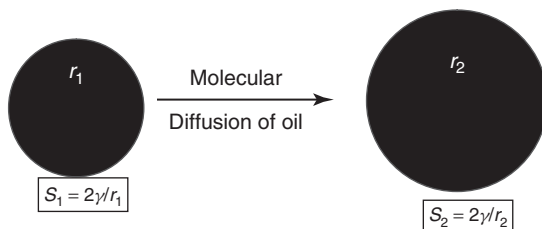


Figure 1.34 Schematic representation of Ostwald ripening.

D is the diffusion coefficient of the disperse phase in the continuous phase and ρ is the density of the disperse phase.

Several methods may be applied to reduce Ostwald ripening [39–41]. (i) Addition of a second disperse phase component that is insoluble in the continuous medium (e.g., squalane). In this case, partitioning between different droplet sizes occurs, with the component having low solubility expected to be concentrated in the smaller droplets. During Ostwald ripening in a two-component system, equilibrium is established when the difference in chemical potential between different size droplets (which results from curvature effects) is balanced by the difference in chemical potential resulting from partitioning of the two components. This effect reduces further growth of droplets. (ii) Modification of the interfacial film at the O/W interface. According to Eq. (1.89), reduction in γ results in reduction of Ostwald ripening rate. By using surfactants that are strongly adsorbed at the O/W interface (i.e., polymeric surfactants) and that do not desorb during ripening (by choosing a molecule that is insoluble in the continuous phase), the rate could be significantly reduced. An increase in the surface dilational modulus $\varepsilon (= d\gamma/d\ln A)$ and decrease in γ would be observed for the shrinking drop, and this tends to reduce further growth.

A-B-A block copolymers such as PHS-PEO-PHS (which is soluble in the oil droplets but insoluble in water) can be used to achieve the above effect. Similar effects can also be obtained using a graft copolymer of hydrophobically modified inulin, namely INUTEC[®] SP1 (ORAFTEI, Belgium). This polymeric surfactant adsorbs with several alkyl chains (which may dissolve in the oil phase) leaving loops and tails of strongly hydrated inulin (polyfructose) chains. The molecule has limited solubility in water and hence it resides at the O/W interface. These polymeric emulsifiers enhance the Gibbs elasticity thus significantly reducing the Ostwald ripening rate.

1.11 Emulsion Coalescence

When two emulsion droplets come in close contact in a floc or creamed layer or during Brownian diffusion, thinning and disruption of the liquid film may occur resulting in eventual rupture. On close approach of the droplets, film thickness fluctuations may occur – alternatively, the liquid surfaces undergo some fluctuations forming surface waves, as illustrated in Figure 1.35.

The surface waves may grow in amplitude and the apices may join as a result of the strong van der Waals attraction (at the apex, the film thickness is the smallest). The same applies if the film thins to a small value (critical thickness for coalescence).

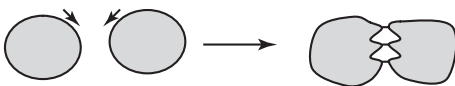


Figure 1.35 Schematic representation of surface fluctuations.

A very useful concept was introduced by Deryaguin and Scherbaker [42] who suggested that a “disjoining pressure” $\pi(h)$ is produced in the film that balances the excess normal pressure

$$\pi(h) = P(h) - P_o \quad (1.92)$$

where $P(h)$ is the pressure of a film with thickness h and P_o is the pressure of a sufficiently thick film such that the net interaction free energy is zero.

$\pi(h)$ may be equated to the net force (or energy) per unit area acting across the film

$$\pi(h) = -\frac{dG_T}{dh} \quad (1.93)$$

where G_T is the total interaction energy in the film.

$\pi(h)$ is made of three contributions due to electrostatic repulsion (π_E), steric repulsion (π_s), and van der Waals attraction (π_A)

$$\pi(h) = \pi_E + \pi_s + \pi_A \quad (1.94)$$

To produce a stable film $\pi_E + \pi_s > \pi_A$, this is the driving force for prevention of coalescence that can be achieved by two mechanisms and their combination: (i) increased repulsion both electrostatic and steric and (ii) dampening of the fluctuation by enhancing the Gibbs elasticity. In general, smaller droplets are less susceptible to surface fluctuations and hence coalescence is reduced. This explains the high stability of nanoemulsions.

Several methods may be applied to achieve the above effects:

- 1) **Use of mixed surfactant films:** In many cases using mixed surfactants, for example, anionic and nonionic or long-chain alcohols, can reduce coalescence as a result of several effects such as high Gibbs elasticity, high surface viscosity, and hindered diffusion of surfactant molecules from the film.
- 2) **Formation of lamellar liquid crystalline phases at the O/W interface:** This mechanism was suggested by Friberg and coworkers [43], who suggested that surfactant or mixed surfactant film can produce several bilayers that “wrap” the droplets. As a result of these multilayer structures, the potential drop is shifted to longer distances thus reducing the van der Waals attraction. A schematic representation of the role of liquid crystals is shown in Figure 1.36 that illustrates the difference between having a monomolecular layer and a multilayer as is the case with liquid crystals.

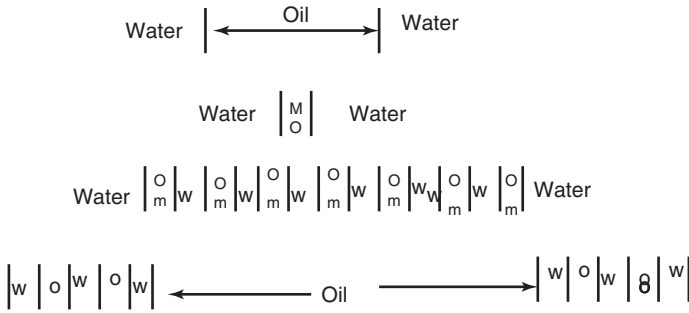
For coalescence to occur, these multilayers have to be removed “two-by-two” and this forms an energy barrier preventing coalescence.

1.11.1

Rate of Coalescence

As film drainage and rupture is a kinetic process, coalescence is also a kinetic process. If one measures the number of particles n (flocculated or not) at time t

$$n = n_t + n_v m \quad (1.95)$$



Upper part monomolecular layer
 Lower part presence of liquid crystalline phases

Figure 1.36 Schematic representation of the role of liquid crystalline phases.

where n_i is the number of primary particles remaining and n is the number of aggregates consisting of m separate particles.

For studying emulsion coalescence, one should consider the rate constant of flocculation and coalescence. If coalescence is the dominant factor, then the rate K follows a first-order kinetics

$$n = \frac{n_o}{Kt} [1 + \exp(-Kt)] \tag{1.96}$$

which shows that a plot of $\log n$ versus t should give a straight line from which K can be calculated.

1.11.2

Phase Inversion

Phase inversion of emulsions can be one of two types: transitional inversion induced by changing the factors that affect the HLB of the system, for example, temperature and/or electrolyte concentration and catastrophic inversion, which is induced by increasing the volume fraction of the disperse phase.

Catastrophic inversion is illustrated in Figure 1.37 that shows the variation of viscosity and conductivity with the oil volume fraction ϕ . As can be seen, inversion occurs at a critical ϕ , which may be identified with the maximum packing fraction. At ϕ_{cr} , η suddenly decreases – the inverted W/O emulsion has a much lower volume fraction. κ also decreases sharply at the inversion point because the continuous phase is now oil.

Earlier theories of phase inversion were based on packing parameters. When ϕ exceeds the maximum packing (~ 0.64 for random packing and ~ 0.74 for hexagonal packing of monodisperse spheres; for polydisperse systems, the maximum packing exceeds 0.74), inversion occurs. However, these theories are not adequate, because many emulsions invert at ϕ values well below the maximum packing as a result of the change in surfactant characteristics with variation of conditions. For example,

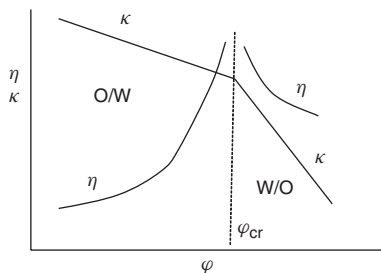


Figure 1.37 Variation of conductivity and viscosity with volume fraction of oil.

when using a nonionic surfactant based on PEO, the latter chain changes its solvation by increase of temperature and/or addition of electrolyte. Many emulsions show phase inversion at a critical temperature (the PIT) that depends on the HLB number of the surfactant as well as the presence of electrolytes. By increasing temperature and/or addition of electrolyte, the PEO chains become dehydrated and finally they become more soluble in the oil phase. Under these conditions, the O/W emulsion will invert to a W/O emulsion. The above dehydration effect amounts to a decrease in the HLB number and when the latter reaches a value that is more suitable for W/O emulsion inversion will occur. At present, there is no quantitative theory that accounts for phase inversion of emulsions.

1.12

Rheology of Emulsions

The rheology of emulsions has many similar features to that of suspensions. However, they differ in three main aspects. (i) The mobile liquid/liquid interface that contains surfactant or polymer layers introduces a response to deformation and one has to consider the interfacial rheology. (ii) The dispersed-phase viscosity relative to that of the medium has an effect on the rheology of the emulsion. (iii) The deformable nature of the dispersed-phase droplets, particularly for large droplets, has an effect on the emulsion rheology at high phase volume fraction ϕ .

When the above factors are considered, one can treat the bulk rheology of emulsions in a similar way as for suspensions and the same techniques used can be applied.

1.12.1

Interfacial Rheology

1.12.1.1 Interfacial Tension and Surface Pressure

A fluid interface in equilibrium exhibits an intrinsic state of tension that is characterized by its interfacial tension γ , which is given by the change in free

energy with area of the interface, at constant composition n_i and temperature T

$$\gamma = \left(\frac{\partial G}{\partial A} \right)_{n_i, T} \quad (1.97)$$

The unit for γ is energy per unit area (mJm^{-2}) or force per unit length (mNm^{-1}), which are dimensionally equivalent.

Adsorption of surfactants or polymers lowers the interfacial tension and this produces a two-dimensional surface pressure π that is given by

$$\pi = \gamma_0 - \gamma \quad (1.98)$$

where γ_0 is the interfacial tension of the “clean” interface (before adsorption) and γ that after adsorption.

1.12.1.2 Interfacial Shear Viscosity

The interface is considered to be a macroscopically planer, dynamic fluid interface. Thus, the interface is regarded as a two-dimensional entity independent of the surrounding three-dimensional fluid. The interface is considered to correspond to a highly viscous insoluble monolayer and the interfacial stress σ_s acting within such a monolayer is sufficiently large compared to the bulk fluid stress acting across the interface, and in this way, one can define an interfacial shear viscosity η_s

$$\sigma_s = \eta_s \dot{\gamma} \quad (1.99)$$

where $\dot{\gamma}$ is the shear rate. η_s is given in surface pascal seconds ($\text{N m}^{-1} \text{s}$) or surface poise (dyne per centimeter second).

It should be mentioned that the surface viscosity of a surfactant-free interface is negligible and it can reach high values for adsorbed rigid molecules such as proteins.

1.12.2

Measurement of Interfacial Viscosity

Many surface viscometers use torsional stress measurements on rotating a ring, disk, or knife-edge (Figure 1.38) within or near to the liquid/liquid interface [44]. This type of viscometer is moderately sensitive; for a disk viscometer, the interfacial shear viscosity can be measured in the range $\eta_s \geq 10^{-2}$ surface Pa s.

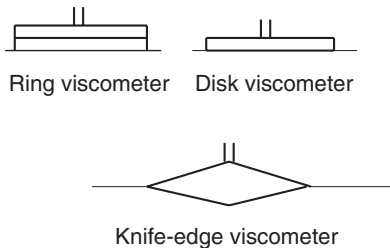


Figure 1.38 Schematic representation of surface viscometers.

The disk is rotated within the plane of the interface with angular velocity ω . A torque is exerted on the disk of radius R by both the surfactant film with surface viscosity η_s and the viscous liquid (with bulk viscosity η) that is given by the expression

$$M = (8/3)R^3\eta\omega + 4\pi R^2\eta_s\omega \quad (1.100)$$

1.12.3

Interfacial Dilational Elasticity

The interfacial dilational (Gibbs) elasticity ε that is an important parameter in determining emulsion stability (reduction of coalescence during formation) is given by the following equation:

$$\varepsilon = \frac{d\gamma}{d \ln A} \quad (1.101)$$

where $d\gamma$ is the change in interfacial tension during expansion of the interface by an amount dA (referred to as *interfacial tension gradient* resulting from nonuniform surfactant adsorption on expansion of the interface).

One of the most convenient methods for measurement of ε is to use a Langmuir trough with two moving barriers for expansion and compression of the interface. Another method for measurement of ε is to use the oscillating bubble technique and instruments are commercially available.

A useful method for measurement of ε is the pulsed drop method [45]. Rapid expansion of a droplet at the end of the capillary from a radius r_1 to r_2 is obtained by application of pressure. The pressure drop within the droplet is measured as a function of time using a sensitive pressure transducer. From the pressure drop, one can obtain the interfacial tension as a function of time. The Gibbs dilational elasticity is determined from values of the time-dependent interfacial tension. Measurement can be made as a function of frequency as illustrated in Figure 1.39 for stearic acid at the decane–water interface at pH = 2.5.

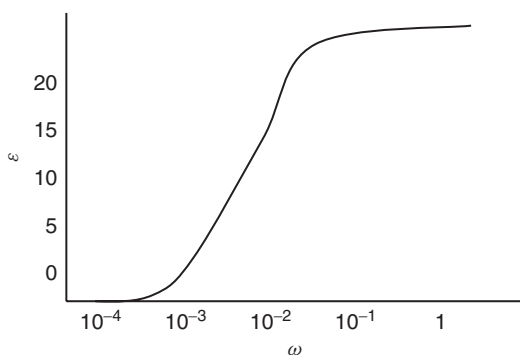


Figure 1.39 Gibbs dilational elasticity versus frequency.

1.12.4

Interfacial Dilational Viscosity

Measurement of the dilational viscosity is more difficult than measurement of the interfacial shear viscosity. This is due to the coupling between dilational viscous and elastic components. The most convenient method for measurement of dilational viscosity is the maximum bubble pressure technique that can be only applied at the A/W interface. According to this technique, the pressure drop across the bubble surface at the instant when the bubble possesses a hemispherical shape (corresponding to the maximum pressure) is due to a combination of bulk viscous, surface tension, and surface dilational viscosity effects, and this allows one to obtain the interfacial dilational viscosity.

1.12.5

Non-Newtonian Effects

Most adsorbed surfactant and polymer coils at the O/W interface show non-Newtonian rheological behavior. The surface shear viscosity η_s depends on the applied shear rate, showing shear thinning at high shear rates. Some films also show Bingham plastic behavior with a measurable yield stress.

Many adsorbed polymers and proteins show viscoelastic behavior and one can measure viscous and elastic components using sinusoidally oscillating surface dilation. For example, the complex dilational modulus ε^* obtained can be split into an “in-phase” (the elastic component ε') and “out-of-phase” (the viscous component ε'') components. Creep and stress relaxation methods can be applied to study viscoelasticity.

1.12.6

Correlation of Emulsion Stability with Interfacial Rheology**1.12.6.1 Mixed Surfactant Films**

Prins *et al.* [46] found that a mixture of SDS and dodecyl alcohol give a more stable O/W emulsion when compared to emulsions prepared using SDS alone. This enhanced stability is due to the higher interfacial dilational elasticity ε for the mixture when compared to that of SDS alone. Interfacial dilational viscosity did not play a major role because the emulsions are stable at high temperature whereby the interfacial viscosity becomes lower.

The above correlation is not general for all surfactant films because other factors such as thinning of the film between emulsion droplets (which depends on other factors such as repulsive forces) can also play a major role.

1.12.6.2 Protein Films

Biswas and Haydon [47] found some correlation between the viscoelastic properties of protein (albumin or arabinic acid) films at the O/W interface and the stability of emulsion drops against coalescence. Viscoelastic measurements were carried

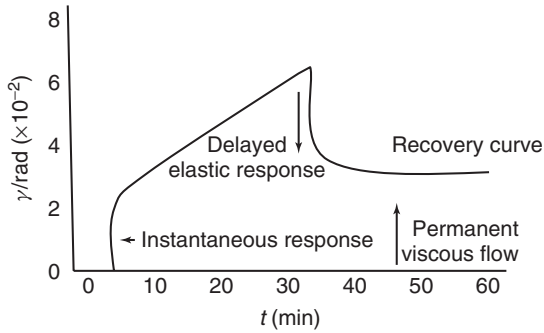


Figure 1.40 Creep curve for protein film at the O/W interface.

out using creep and stress relaxation measurements (using a specially designed interfacial rheometer). A constant torque or stress σ (mN m^{-1}) was applied, and the deformation γ was measured as a function of time for 30 min. After this period, the torque was removed and γ (which changes sign) was measured as a function of time to obtain the recovery curve. The results are illustrated in Figure 1.40.

From the creep curves, one can obtain the instantaneous modulus $G_o(\sigma/\gamma_{\text{int}})$ and the surface viscosity η_s from the slope of the straight line (which gives the shear rate) and the applied stress. G_o and η_s are plotted versus pH as shown in Figure 1.41. Both show increase with increase in pH reaching a maximum at $\sim\text{pH} = 6$ (the isoelectric point of the protein) at which the protein molecules show maximum rigidity at the interface.

The stability of the emulsion was assessed by measuring the residence time t of several oil droplets at a planer O/W interface containing the adsorbed protein. Figure 1.41 shows the variation of $t_{1/2}$ (time taken for half the number of oil droplets to coalesce with the oil at the O/W interface) with pH. Good correlation between $t_{1/2}$ and G_o and η_s is obtained.

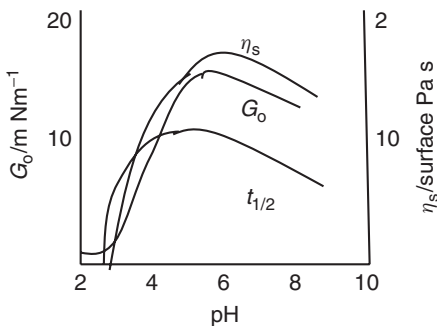


Figure 1.41 Variation of $t_{1/2}$ and G_o and η_s with pH.

Biswas and Haydon [47] derived a relationship between coalescence time τ and surface viscosity η_s , instantaneous modulus G_o , and adsorbed film thickness h

$$\tau = \eta_s \left[3C' \frac{h^2}{A} - \frac{1}{G_o} - \phi(t) \right] \quad (1.102)$$

where $3C'$ is a critical deformation factor, A is the Hamaker constant, and $\phi(t)$ is the elastic deformation per unit stress.

Equation (1.102) shows that τ increases with increase of η_s , but most importantly, it is directly proportional to h^2 . These results show that viscoelasticity is necessary but not sufficient to ensure stability against coalescence. To ensure stability of an emulsion, one must make sure that h is large enough and film drainage is prevented.

1.13

Bulk Rheology of Emulsions

For rigid (highly viscous) oil droplets dispersed in a medium of low viscosity such as water, the relative viscosity η_r of a dilute (volume fraction $\phi \leq 0.01$) O/W emulsion of noninteracting droplets behaves as “hard spheres” (similar to suspensions) [48, 49].

In the above case, η_r is given by the Einstein equation [50]

$$\eta_r = 1 + [\eta]\phi \quad (1.103)$$

where $[\eta]$ is the intrinsic viscosity that is equal to 2.5 for hard spheres.

For droplets with low viscosity (comparable to that of the medium), the transmission of tangential stress across the O/W interface, from the continuous phase to the dispersed phase, causes liquid circulation in the droplets. Energy dissipation is less than that for hard spheres and the relative viscosity is lower than that predicted by the Einstein equation.

For an emulsion with viscosity η_i for the disperse phase and η_o for the continuous phase [48]

$$[\eta] = 2.5 \left(\frac{\eta_i + 0.4\eta_o}{\eta_i + \eta_o} \right) \quad (1.104)$$

Clearly when $\eta_i \gg \eta_o$, the droplets behave as rigid spheres and $[\eta]$ approaches the Einstein limit of 2.5. In contrast if $\eta_i \ll \eta_o$ (as is the case for foams), $[\eta] = 1$.

In the presence of viscous interfacial layers, Eq. (1.104) is modified to take into account the surface shear viscosity η_s and surface dilational viscosity μ_s

$$[\eta] = 2.5 \left(\frac{\eta_i + 0.4\eta_o + \xi}{\eta_i + \eta_o + \xi} \right) \quad (1.105)$$

$$\xi = \frac{(2\eta_s + 3\mu_s)}{R} \quad (1.106)$$

R is the droplet radius.

When the volume fraction of droplets exceeds the Einstein limit, that is, $\phi > 0.01$, one must take into account the effect of Brownian motion and interparticle interactions. The smaller the emulsion droplets, the more important the contribution of Brownian motion and colloidal interactions. Brownian diffusion tends to randomize the position of colloidal particles, leading to the formation of temporary doublets, triplets, and so on. The hydrodynamic interactions are of longer range than the colloidal interactions, and they come into play at relatively low volume fractions ($\phi > 0.01$) resulting in ordering of the particles into layers and tending to destroy the temporary aggregates caused by the Brownian diffusion. This explains the shear thinning behavior of emulsions at high shear rates.

For the volume fraction range $0.01 < \phi < 0.2$, Batchelor [51] derived the following expression for a dispersion of hydrodynamically interacting hard spheres

$$\eta_r = 1 + 2.5\phi + 6.2\phi^2 + \nu\phi^3 \quad (1.107)$$

The second term in Eq. (1.107) is the Einstein limit, the third term accounts for hydrodynamic (two-body) interaction, while the fourth term relates to multibody interaction.

At higher volume fractions ($\phi > 0.2$), η_r is a complex function of ϕ and the $\eta_r - \phi$ curve is schematically shown in Figure 1.42. This curve is characterized by two asymptotes $[\eta]$ the intrinsic viscosity and ϕ_p the maximum packing fraction.

A good semiempirical equation that fits the curve is given by Dougherty and Krieger [52, 53]

$$\eta_r = \left(1 - \frac{\phi}{\phi_p}\right)^{-[\eta]\phi_p} \quad (1.108)$$

1.13.1

Analysis of the Rheological Behavior of Concentrated Emulsions

When considering the rheology of concentrated emulsions (without deformation of the emulsion drops), one should attempt to find an expression for the fourth term in ϕ^3 of Eq. (1.107). Unfortunately, there is no theoretical rigorous treatment of this term and only semiempirical equations are available [54, 55] for the case of intermediate volume fractions.

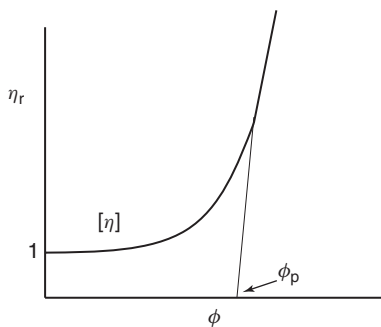


Figure 1.42 $\eta_r - \phi$ curve.

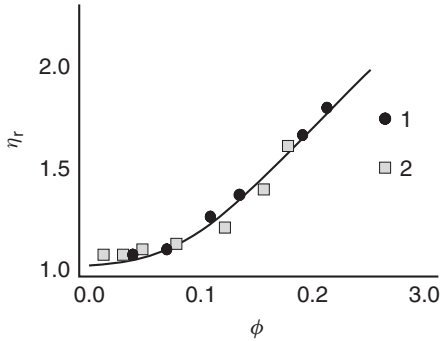


Figure 1.43 Comparison of experimental data of the concentration dependence of different emulsions with some theoretical predictions.

Two models were proposed by Pal [56] that are described by the following expressions

$$\eta_r \left[\frac{2\eta_r + 5\lambda}{2 + 5\lambda} \right]^{1/2} = \exp \left[\frac{2.5\varphi}{1 - (\varphi/\varphi^*)} \right] \quad (1.109)$$

$$\eta_r \left[\frac{2\eta_r + 5\lambda}{2 + 5\lambda} \right]^{1/2} = [1 - (\varphi/\varphi^*)]^{-25\varphi^*} \quad (1.110)$$

where λ is the ratio of viscosities of disperse drops and continuous medium and φ^* is the limit of closest packing of drops in free space (as in suspensions), although it was used as a free fitting factor.

The above models describe rather well experimental data for various real emulsions in a wide concentration range as illustrated in Figure 1.43.

The increase of the concentration of drops in emulsions results not only in an increase in viscosity at low shear rates (the limiting residual Newtonian viscosity $\eta(0)$) but also in the appearance of strong non-Newtonian effects, that is, a shear rate dependence of the apparent viscosity. This is illustrated in Figure 1.44 that shows the variation of viscosity with applied stress [54]. This figure shows the remarkable transition from an almost Newtonian behavior at low stresses to an anomalous flow with pronounced non-Newtonian effects.

Another example of the changes in the character of rheological properties just close to the upper boundary of the concentration domain, that is, when approaching the state of closest packing of spherical drops is shown in Figure 1.45 for a water-in-oil emulsion [57, 58].

As seen in Figures 1.44 and 1.45, the approach to the limit of high concentration and transition beyond the closest packing of nondeformable spherical drops leads to principle changes in the rheological properties. The Newtonian viscous flow is replaced by a viscoplastic behavior with jumplike decrease (by several orders of magnitude) in the apparent viscosity in a narrow range of applied stresses. The jump in the apparent viscosity at some shear stress is the reflection of the rupture of the structure, and this stress may be treated as a yield stress.

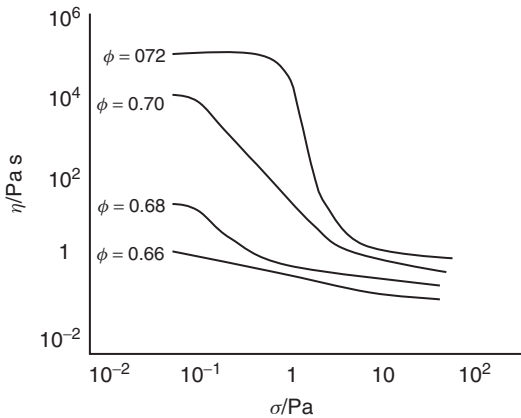


Figure 1.44 Flow curves of model “oil-in-water” emulsion (average drop size of 4.6 μm) at various volume fractions.

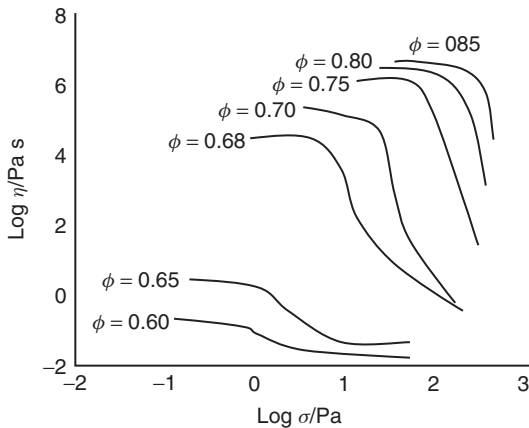


Figure 1.45 Flow curves of “water-in-oil” emulsions when approaching the concentration limit corresponding to the closest packing of spherical drops.

At high volume fractions ($\phi > 0.6$), there is a significant effect of the average droplet diameter (volume to surface ratio d_{32}). The drop size influences the volume to surface ratio, and this leads to a more pronounced effect of the flow inside the drops. This phenomenon becomes more significant when approaching to the upper boundary of intermediate concentrations. This is illustrated in Figures 1.46 and 1.47 that show the variation of viscosity with volume fraction for emulsions with various droplet diameters [56–58]. In the low-volume fraction regime (Figure 1.46), that is, at $\phi < 0.6$, there is hardly any effect of the droplet diameter on the viscosity of the emulsion. However, in the high-volume fraction regime ($\phi > 0.6$), reduction in droplet diameter results in a significant increase of the viscosity.

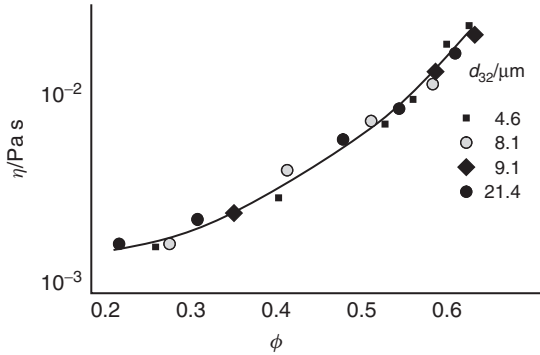


Figure 1.46 Viscosity–volume fraction curves for emulsions with different droplet diameters and at low-volume fractions ($\phi < 0.6$).

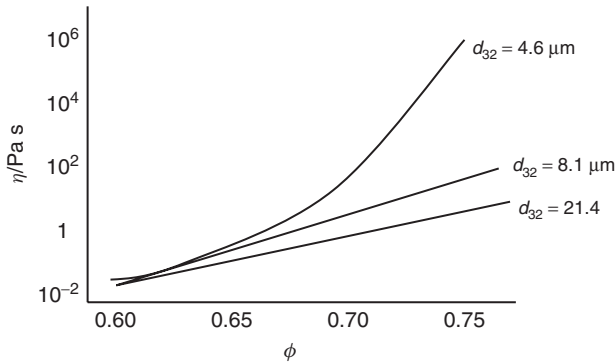


Figure 1.47 Viscosity–volume fraction curves for emulsions with different droplet and at high-volume fractions ($\phi < 0.6$).

Another rheological behavior of concentrated emulsions is the presence of thixotropy. The interfacial layers in the closely arranged drops can produce a certain type of structure, which is destroyed by deformation but restored at rest.

Another rheological behavior of concentrated emulsions is the presence of thixotropy. The interfacial layers in the closely arranged drops can produce some kind of structure, which is destroyed by deformation and restores at rest. The interaction between drops and evolution of their shape in flow can also result in viscoelastic effects as is discussed below.

1.14

Experimental $\eta_r - \phi$ Curves

Experimental results of $\eta_r - \phi$ curves were obtained for paraffin O/W emulsions stabilized with an A-B-C surfactant consisting of nonyl phenol (B), 13 mol propylene oxide stabilized with the surfactant containing 27 EO (the volume medium diameter

of the droplets is $3.5\ \mu\text{m}$). The calculations based on the Dougherty–Krieger equation are also shown in the same figure.

1.14.1

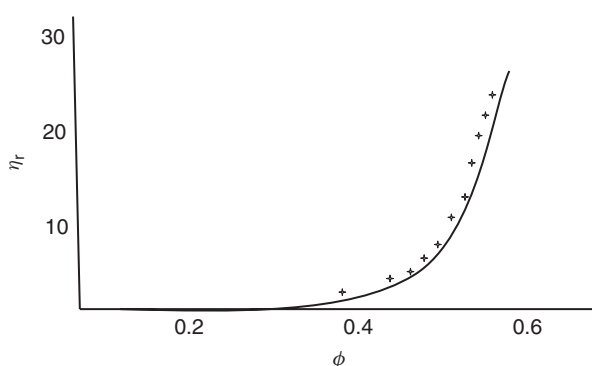
Experimental $\eta_r - \phi$ Curves

Experimental results for $\eta_r - \phi$ curves were obtained for paraffin O/W emulsions [48] stabilized with an A-B-C surfactant consisting of nonyl phenol (B), 13 mol of propylene oxide (C), and PEO with 27, 48, 80, and 174 mol EO. As an illustration, Figure 1.48 shows the results for an emulsion stabilized with the surfactant containing 27 EO 9 (the volume median diameter of the droplets was $3.5\ \mu\text{m}$). Calculations based on the Dougherty–Krieger equation are also shown in the same figure. In these calculations, $[\eta] = 2.5$ and ϕ_p was obtained from a plot of $\eta^{-1/2}$ versus ϕ and extrapolation of the straight line to $\eta^{-1/2} = 0$. The value of ϕ_p was 0.73 (which is higher than the maximum random packing of 0.64) as a result of the polydispersity of the emulsion. The results using the other three surfactants showed the same trend; the experimental $\eta_r - \phi$ curves are close to those calculated using the Dougherty–Krieger equation indicating that these emulsions behave as hard spheres.

1.14.2

Influence of Droplet Deformability

The influence of droplet deformability on emulsion rheology was investigated by Saiki *et al.* [59] by comparing the $\eta_r - \phi$ curves of hard spheres of silica with two dimethylsiloxane poly-dimethylsiloxane (PDMS) emulsions with low (PDMS 0.3) and high deformability (PDMS 0.45) (by controlling the proportion of cross-linking agent for the droplets; 0.3 low and 0.45 high cross-linking agent). The $\eta_r - \phi$ curves for the three systems are shown in Figure 1.49. The $\eta_r - \phi$ curve for silica can be



+ experimental results; Full line calculated curve using Dougherty-Krieger equation

Figure 1.48 Experimental and theoretical $\eta_r - \phi$ curve.

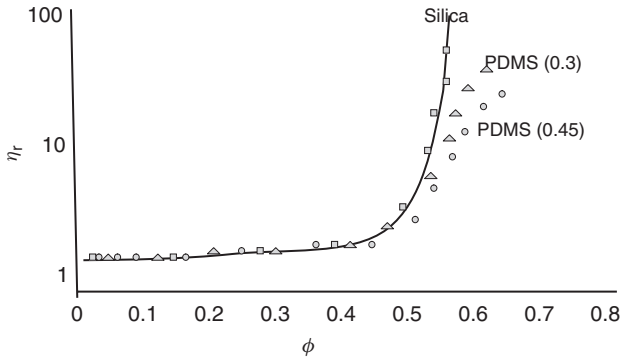


Figure 1.49 η_r - ϕ curves for silica and two PDMS emulsions.

fitted by the Dougherty–Krieger equation over the whole volume fraction range indicating typical hard sphere behavior. The $\eta_r - \phi$ curve for the less deformable PDMS deviates from the hard sphere curve at $\phi = 0.58$. The $\eta_r - \phi$ curve for the more deformable PDMS deviates from the hard sphere curve at $\phi = 0.40$. This clearly shows that the deformation of the “soft” droplets occurs at relatively low-volume fraction.

1.15

Viscoelastic Properties of Concentrated Emulsions

The viscoelastic properties of emulsions can be investigated using dynamic (oscillatory) measurements. A sinusoidal strain with amplitude γ_0 is applied on the system at a frequency ω (rad s^{-1}), and the stress σ (with amplitude σ_0) is simultaneously measured. From the time shift Δt between the sine waves of strain and stress, one can measure the phase angle shift δ ($\delta = \Delta t\omega$).

From σ_0 , γ_0 , and δ , one can obtain the complex modulus G^* , the storage modulus G' (the elastic component), and the loss modulus G'' (the viscous component).

G^* , G' , and G'' are measured as a function of strain amplitude to obtain the linear viscoelastic region and then as a function of frequency (keeping γ_0 in the linear region). As an illustration, Figure 1.50 shows the results for an O/W emulsion at $\phi = 0.6$ (the emulsion was prepared using an A-B-A block copolymer of PEO, A and PPO, B with an average of 47 PO units and 42 EO units [49]).

The results of Figure 1.50 are typical for a viscoelastic liquid. In the low-frequency regime (<1 Hz), $G'' > G'$. As the frequency ω increases, G' increases, at a characteristic frequency ω^* (the cross-over point), G' becomes higher than G'' , and at high frequency, it becomes closer to G^* . G'' increases with increase in frequency reaching a maximum at ω^* after which it decreases with further increase in frequency.

From ω^* , one can calculate the relaxation time t^*

$$t^* = \frac{1}{2\pi\omega^*} \quad (1.111)$$

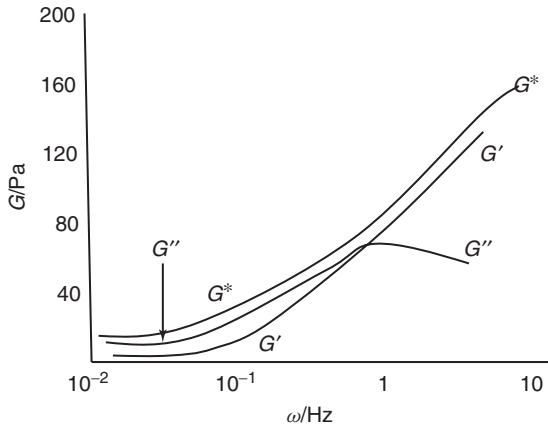


Figure 1.50 Variation of G^* , G' , and G'' with frequency ω/Hz .

For the above value of $\phi (= 0.6)$, $t^* = 0.12$ s. t^* increases with increase in ϕ and this reflects the stronger interaction with increase in ϕ .

To obtain the onset of strong elastic interaction in emulsions, G^* , G' , and G'' (obtained in the linear viscoelastic region and high frequency, e.g., 1 Hz) are plotted versus the volume fraction of the emulsion ϕ . One should make sure that the droplet size distribution in all emulsions is the same. The most convenient way is to prepare an emulsion at the highest possible ϕ (e.g., 0.6), and this emulsion is then diluted to obtain various ϕ values. Droplet size analysis should be obtained for each emulsion to make sure that the size distribution is the same.

Figure 1.51 shows the plots for G^* , G' , and G'' versus ϕ . At $\phi < 0.56$, $G'' > G'$ whereas at $\phi > 0.56$, $G' > G''$ — $\phi = 0.56$ is the onset of predominantly elastic interaction and this reflects the small distance of separation between the droplets.

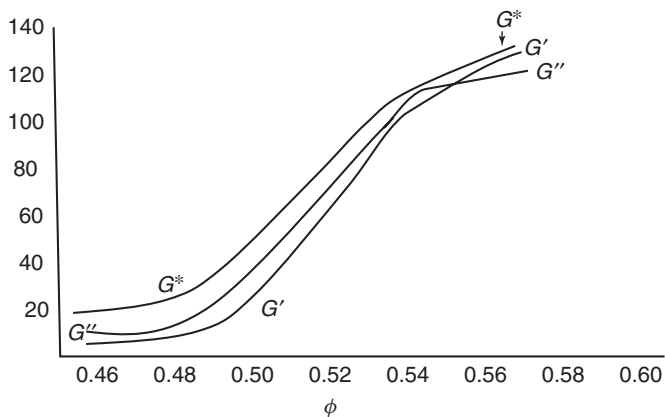


Figure 1.51 Variation of G^* , G' , and G'' with ϕ .

1.15.1

High Internal Phase Emulsions (HIPEs)

The maximum packing fraction ϕ^* of nondeformable droplets in an emulsion is in the region of 0.71–0.75, depending on the droplet size distribution and arrangement of drops in space. However, some emulsion systems can exceed this maximum, that is, with $\phi > \phi^*$ and these are referred to as high internal phase emulsions (HIPEs). To achieve this, deformation of the spherical droplets must take place via compression of a dispersion resulting in transformation of the spherical droplets into tightly packed polygon-shaped particles that occupy the space. These systems have wide application in cosmetics, food stuffs, and emulsion explosives.

The general thermodynamic approach to understanding the nature and properties of HIPEs was proposed by Princen [60]. According to this approach, HIPEs are created by application of outer pressure that compresses the drops and transform them from spheres to polygons. This outer pressure is equivalent to the osmotic pressure Π acting inside the thermodynamic system. The work produced by this pressure when creating an HIPE is equal to the stored energy by the increase of droplet surface area S due to changes in shape. This equality is given by the following expression:

$$-\Pi dV = \sigma dS \quad (1.112)$$

where σ is the interfacial tension.

Equation (1.112) shows that the osmotic pressure for decreasing the volume ΠdV is equal to the work needed for creating additional new surface dS .

Substituting the expression for concentration gives the equation for the osmotic pressure as a function of volume fraction ϕ and change in surface area S (reduced by the volume V)

$$\Pi = \sigma \phi^2 \frac{d(S/V)}{d\phi} \quad (1.113)$$

The stored surface energy serves as a source of elasticity of the HIPE, which is observed in shear deformation [61–64]. The experimental evidence of this conception is seen in close correlation between the concentration dependence of the shear elastic modulus G and osmotic pressure Π as shown in Figure 1.52. The experimental data of Figure 1.52 are reduced by the Laplace pressure (σ/R).

Using a reduction factor, (σ/R) reflects the proposed conception of elasticity of HIPEs as a consequence of the increase of surface energy on compression of a drop [61–63]. This approach presumes that both G and Π are inversely proportional to droplet size. The concentration dependence of elasticity should be the product $\phi^{1/3}(\phi - \phi^*)$ or $\phi(\phi - \phi^*)$ as discussed by Princen and Kiss [65]. The solidlike properties of HIPEs can be observed when $\phi > \phi^*$. The elasticity of HIPEs can be illustrated from measurement of the modulus as a function of frequency. This is shown in Figure 1.53 for a model emulsion of monodisperse droplets ($R = 500$ nm) of poly(dimethyl siloxane) in water at a volume fraction ϕ of 0.98 [65].

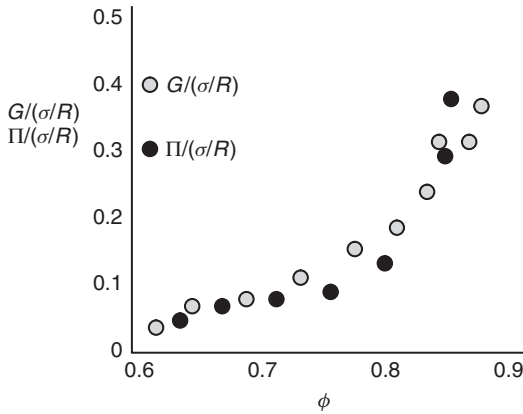


Figure 1.52 Correlation between the elastic modulus (open circles) and osmotic pressure (closed circles) for HIPEs.

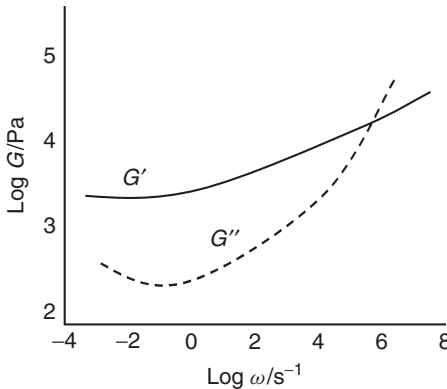


Figure 1.53 Variation of the storage modulus G' and loss modulus G'' with frequency for poly(dimethyl siloxane) emulsion ($r = 600$ nm) at $\phi = 0.98$.

The elastic modulus G' shows little dependency on frequency up to 10^2 s^{-1} indicating that the HIPE behaves as a linear elastic material. However, G' increases at very high frequencies and this effect is attributed to a mechanical glass transition of the emulsion as a viscoelastic material [65].

Further rheological measurements [66] indicated that HIPEs show nonlinear viscoelastic as well as viscous behavior. This is illustrated in Figure 1.54 that shows the variation of the complex modulus with stress for highly concentrated emulsions at various volume fractions. It can be seen that the modulus remains virtually constant with the increase in stress, but at a critical stress, it shows a rapid decrease indicating “softening” of the structure at high stress values. Such behavior is typical for “structured” colloidal dispersions that undergo destruction of this structure when the stress exceeds a critical value.

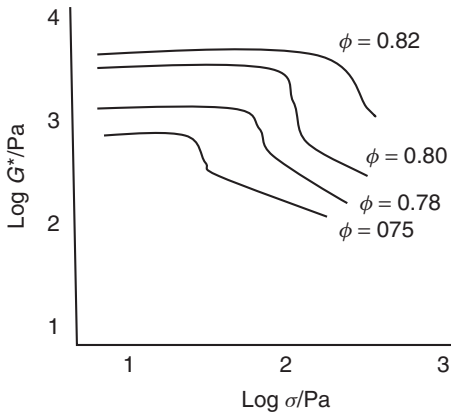


Figure 1.54 Variation of complex modulus with applied stress for highly concentrated (cosmetic grade) water-in-oil emulsions.

It is important to compare the amplitude dependence of the elastic (storage) modulus G' and the viscous (loss) modulus G'' under conditions of large deformation. As mentioned earlier, HIPEs behave as elastic systems with $G' > G''$. However, at high amplitudes, a solidlike to liquidlike behavior is observed and at a critical strain γ^* (to be referred to as the *melting strain*) $G' = G''$ and this can be considered as a measure of the point of rupture of the materials structure. Above γ^* , $G'' > G'$.

Some authors [67] observed structure formation with increasing strain amplitude, a phenomenon analogous to negative (anti-) thixotropy.

The non-Newtonian behavior of HIPEs can also be demonstrated from flow curves [68] as illustrated in Figure 1.55 for W/O emulsion (liquid explosive) at various volume fractions of HIPEs. As can be seen in Figure 1.55, the yield values show a large increase with a small increase in the volume fraction of the emulsions.

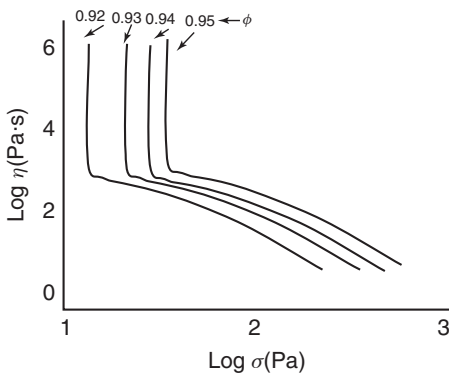


Figure 1.55 Flow curves of highly concentrated water-in-oil emulsions (liquid explosives).

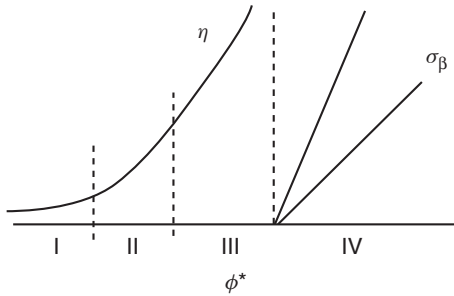


Figure 1.56 General trends of rheological properties of emulsions in the whole volume fraction range.

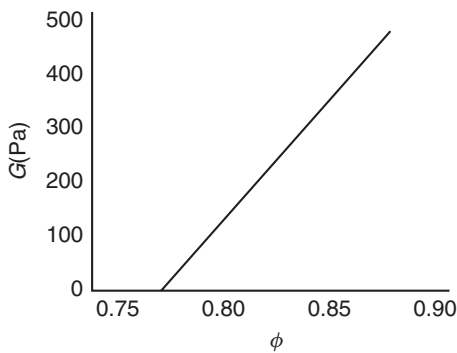


Figure 1.57 Variation of elastic modulus G with volume fraction ϕ .

A schematic representation of the evolution of rheological properties of emulsions from dilute ($\phi \ll 1$) to highly concentrated emulsions ($\phi > \phi^*$) is shown in Figure 1.56 [58]. The transition into the domain of highly concentrated emulsions is accompanied by change in the volume fraction dependence of the rheological properties and the influence of droplet size. This is illustrated in Figures 1.57 and 1.58, which show the variation of elastic modulus G and yield value σ_β with volume fraction ϕ at values above ϕ^* . This linear dependence of G and σ_β on ϕ is consistent with Princen and Kiss [65] discussed earlier.

The influence of droplet size on the viscosity of concentrated emulsions was investigated by Pal [69] who showed that the viscosity of smaller droplets is higher than that of larger droplets at the same volume fraction. This is illustrated in Figure 1.59, which shows the flow curves for an emulsion with $\phi = 0.76$ at two droplet sizes of 12 and 30 μm . In addition to the higher viscosity of the emulsion with the smaller size, the latter shows a more pronounced non-Newtonian effect when compared with the emulsion with the larger size.

The dependence of elastic modulus on droplet diameter can be approximated by the following equation:

$$G = ad_{32}^{-2} \quad (1.114)$$

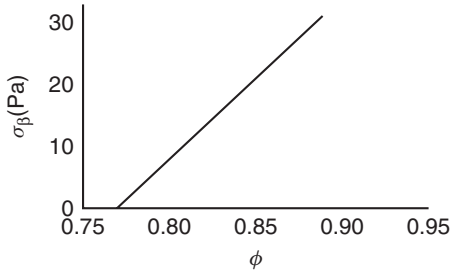


Figure 1.58 Variation of yield stress σ_β with volume fraction ϕ .

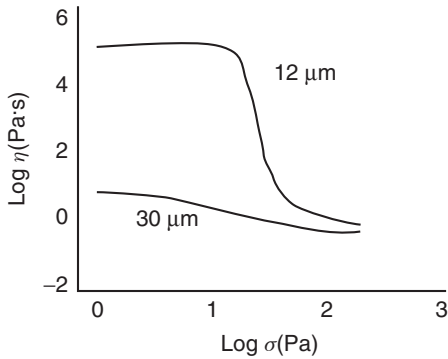


Figure 1.59 Flow curves for concentrated emulsion ($\phi = 0.75$) with two different droplet sizes.

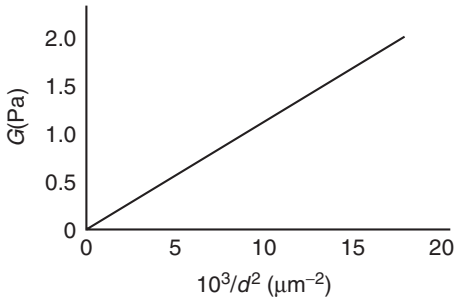


Figure 1.60 Dependence of elastic modulus on average droplet size for highly concentrated emulsions.

Equation (1.114) shows that a plot of G versus $(1/d^2)$ should give a straight line as illustrated in Figure 1.60.

It is worth mentioning that according to the generally accepted Princen [60], Mason *et al.* [63] theory of the dependence of G on d was always considered as reciprocal linear (but not squared) as it follows from the basic concept of elasticity of HIPES discussed previously.

1.15.2

Deformation and Breakup of Droplets in Emulsions during Flow

During flow, the emulsion drops undergo deformation (from spherical to ellipsoidal shape), which is then followed by break up to smaller drops. The driving force for drop deformation is the shear stress, and such deformation is resisted by the interfacial tension as determined by the Laplace pressure. Thus, the morphology of a drop is determined by the ratio of stress to the Laplace pressure, that is, the capillary number Ca given by the following expression:

$$Ca = \frac{\eta_o \dot{\gamma}}{\sigma/R} \quad (1.115)$$

where η_o is the viscosity of the medium, $\dot{\gamma}$ is the shear rate, σ is the interfacial tension, and R is the droplet radius.

The degree of anisotropy D of a deformed drop is based on the classical Taylor model for the viscosity of dilute emulsions [70]

$$D = \frac{16 + 19\lambda}{16(\lambda + 1)} Ca \quad (1.116)$$

where λ is the ratio of viscosity of disperse phase and disperse medium.

For a moderately concentrated emulsion, one must take into account the dynamic interaction between drops and D is given by the following expression [71]:

$$D = \left[\frac{16 + 19\lambda}{16(\lambda + 1)} \right] \left[1 + \frac{5(2 + 5\lambda)}{4(\lambda + 1)} \varphi \right] Ca \quad (1.117)$$

A successful method for obtaining experimental results at various emulsion volume fractions is based on modification of the capillary number whereby the viscosity of the medium η_o is replaced by the “mean field” viscosity, that is, the viscosity of the emulsion as a whole η_{em}

$$Ca_m = \frac{\eta_{em} \dot{\gamma}}{\sigma/R} \quad (1.118)$$

A plot of D versus Ca_m is shown in Figure 1.61 for emulsions with different volume fractions. All results fall on the same line confirming the validity of Eq. (1.118).

The connection between the shape of the droplet and the whole complex behavior of emulsions was established in a series of publications [71–77] for various flow geometries. The final results were obtained in an analytical form. The shear stress in steady flow is expressed as a function of shear rate and capillary number.

The shear stress τ is related to Ca , ratio of viscosities of the disperse phase and medium λ , and volume fraction ϕ of the oil by the following expression:

$$\tau = \frac{2KCa f_1 f_2^2}{3(Ca^2 + f_1^2)} \quad (1.119)$$

where f_1 and f_2 are given by the following expressions:

$$f_1 = \frac{40(\lambda + 1)}{(3 + 2\lambda)(16 + 9\lambda)} \quad (1.120)$$

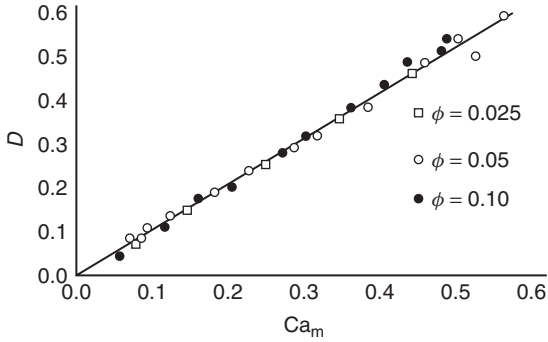


Figure 1.61 Variation of D with Ca_m for emulsions with various volume fractions.

$$f_2 = \frac{5}{3 + 2\lambda} \quad (1.121)$$

The factor K represents the influence of volume fraction on the viscosity

$$K = \left(\frac{6\sigma}{5R}\right) \frac{(\lambda + 1)(3 + \lambda)\varphi}{5(\lambda + 1) - 5(2 + 5\lambda)\varphi} \quad (1.122)$$

The problem of calculating the droplet deformation in a flow of viscous liquid was rigorously formulated by Maffettone and Minale [78]. This deformation consists of the transition from spherical to ellipsoidal shape. The exact solution of this problem was given by Wetzel and Tucker [79] (without taking into account the interfacial tension) and later by Jackson and Tucker [80] who proposed a complete solution including the influence of all factors affecting the shape of a drop. A comparison between the theoretical prediction of the dependence of D on Ca and the experimental results [80] is shown in Figure 1.62.

The deformation of drops in flow from spherical to ellipsoidal shape influences the viscosity of the emulsion [81]. This is confirmed by measurement of the viscosity of an emulsion (water in viscous alkyd resin) at various shear rates. In the low

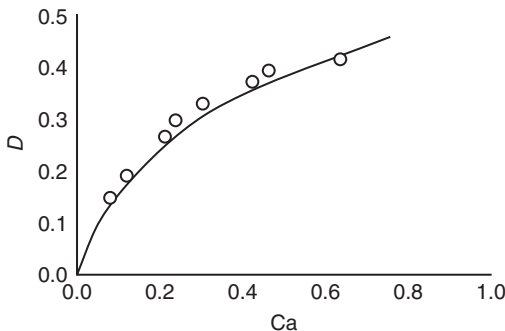


Figure 1.62 Comparison of theoretical prediction of dependence of droplet deformation on capillary number in viscous liquid (solid line) with experimental results (circles).

shear rate regime (where no deformation occurs), the viscosity–volume fraction curve is very close to that of a suspension. However, in the high shear rate regime where deformation of the drops occurs as a result of the low viscosity ratio λ , a non-Newtonian flow is observed and the volume fraction dependence of viscosity is given by the following empirical equation:

$$\eta = \eta_o(1 - \varphi) \quad (1.123)$$

Equation (1.123) shows that the viscosity of the emulsion in the high shear rate regime is lower than that of the medium.

The above problem of calculating the deformation of a drop in a flow is considered without taking into account inertia, that is, at very low Reynolds number. Estimations show that the increase of Reynolds number enhances the impact of inertia, which in turn leads to stronger deformation of the drop and consequently to the growth of stresses in the interfacial layer [82]. It also influences the stability of the drop, which is determined by surface stresses.

The possibility of drop breakup is determined by the balance of the outer stress created by the flow of liquid around the drop (given by the product of the viscosity and shear rate $\eta_o\dot{\gamma}$) and the Laplace pressure (σ/R). Thus, the determining factor for drop stability is a critical value for the capillary number Ca^* that depends on the ratio of the viscosities of disperse droplets and medium λ . The value of Ca^* decreases with increase of λ in the domain $\lambda < 1$ and Arcivos [83] expressed the variation of Ca^* with λ (at low values) by

$$Ca^* = 0.054\lambda^{-2/3} \quad (1.124)$$

Complete results were obtained by Grace [84] who examined both simple shear and two-dimensional extension in the full range of λ values as illustrated in Figure 1.63.

Figure 1.63 shows two interesting results, namely, a minimum in Ca^* of 0.4 when $\lambda = 1$ (i.e., when the viscosities of the disperse phase and medium are equal) and the absence of drop break-up in laminar flow when $\lambda > 4$ (i.e., drops of high viscosity).

The results of systematic investigation of single droplet breakup are shown in Figure 1.64. The experiential data are in reasonable agreement with the theoretical

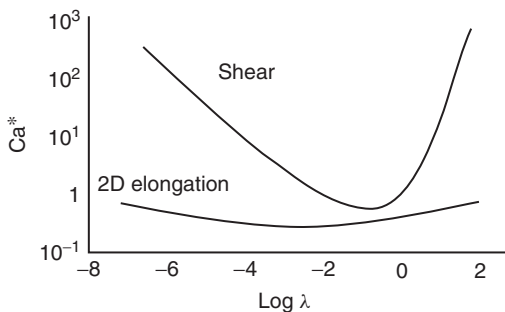


Figure 1.63 Dependence of Ca^* on λ in simple shear and two-dimensional extensional flow.

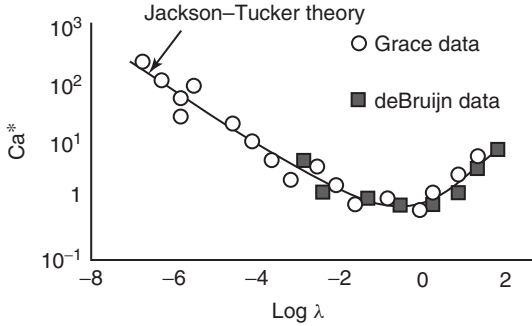


Figure 1.64 Correlation of theoretical dependence of Ca^* on λ (solid line) with experimental data (circles and squares) in laminar simple shear.

prediction of Jackson and Tucker [80]. The *breakup conditions* are defined as the limit of their deformation as discussed above. It is assumed that when a deformation results in some steady state of a drop, then this rate of deformation is less than that corresponding to the critical value Ca^* . The calculations show that droplet deformation becomes continuous without limit, which means that the drop breaks when $Ca > Ca^*$.

The critical conditions for droplet breakup in a viscoelastic medium are different from a purely viscous liquid. Surface stresses at the interface can vary and are a function of the Reynolds number and the Weissenberg number (ratio of characteristic time of outer action and inner relaxation). Numerical modeling demonstrated that the capillary number increases with increasing the Weissenberg number, that is, enhancement of the viscoelasticity of the medium [85].

The above discussion refers to the case of single drops. However, in concentrated emulsions (practical systems), modifications are needed to take into account the droplet–droplet interactions. A convenient method is to modify the definition of Ca^* and λ by substituting the viscosity of the medium by that of the emulsion (mean field approximation). In this way, the modified viscosity ratio λ_m is given by

$$\lambda_m = \frac{\eta_{dr}}{\eta_{em}} \quad (1.125)$$

The results of experimental studies discussed in terms of the function $Ca_m^*(\lambda_m)$ are shown in Figure 1.65 for emulsions with a wide volume fraction range (up to $\phi = 0.7$). The influence of volume fraction is clearly shown in Figure 1.66, which shows plots of the critical shear rate of breakup as a function of reciprocal radius. The higher the value of ϕ , the lower the shear rate required for breakup of the drops. This is consistent with the increase of stress with increasing ϕ .

The drop breakup at a given shear rate can continue up to a limiting value R_{lim} because the capillary number decreases with the decrease of radius and finally it becomes less than the critical value Ca^* . This is illustrated in Figure 1.67, which shows the dependence of R_{lim} on shear rate. A parabolic relationship is obtained

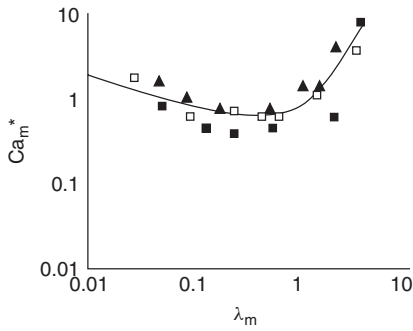


Figure 1.65 Condition of breakup for silicone oil-in-water emulsions at different oil volume fractions (0–0.7).

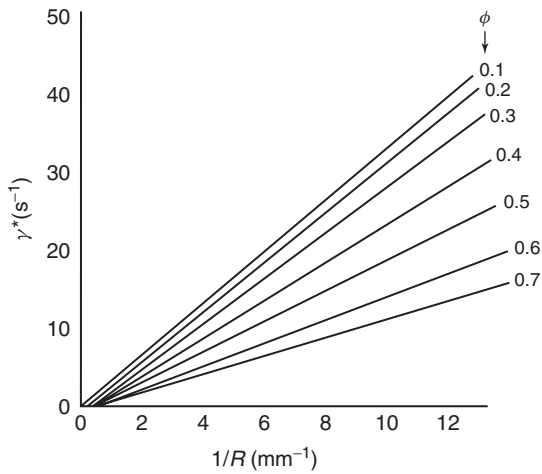


Figure 1.66 Dependence of the critical shear rate corresponding to break up on droplet size for emulsions at different oil volume fractions.

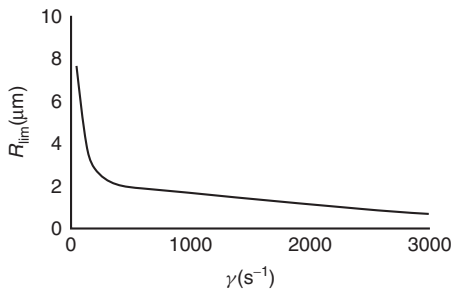


Figure 1.67 Dependence of droplet size (as a result of laminar shearing) on the shear rate for silicone oil-in-water emulsions ($\phi = 0.7$).

that is represented by the following scaling law [86]:

$$R_{\text{lim}} = C \frac{\sigma}{\eta \dot{\gamma}} \quad (1.126)$$

The factor C is of the order 1 and this reflects the critical value of the capillary number.

It is essential that all theoretical models and experiential results must be under conditions of laminar flow. The transition to higher Reynolds number (>2000), that is, under turbulent regime makes the picture of breakup of droplets in emulsions more complicated. The basic problem is the presence of large fluctuations of local velocities and stresses, which makes the theoretical analysis much more complicated when compared to the case of laminar flow.

Generally speaking, there are two regimes for turbulent flow, namely, turbulent inertial (TI) and “turbulent viscous” (TV). The differences between them are related to the ratio of characteristic sizes of liquid droplets and the turbulent vortex [87]. The minimum droplet size in the TI regime depends on the ratio of the dynamic fluctuation (breakup of a droplet) and surface tension, while for TV regime, the breakup of droplets occur under shear stresses across the continuous medium.

Vankova *et al.* [88] showed that the maximum size of a droplet in the TI regime, $d_{\text{TI,max}}$ is given by the following expression:

$$d_{\text{TI,max}} = A_1 (\varepsilon^{-2/5} \sigma^{3/5} \rho_c^{-3/5}) = A_1 d_k \quad (1.127)$$

where A_1 is a factor that is of the order 1, ε is the intensity of energy dissipation characterizing the dynamic situation in a flow, and ρ_c is the density of the continuous phase. The term in brackets designated as d_k is a characteristic length.

The maximum size of a drop in the TV regime, $d_{\text{TV,max}}$, is determined by the viscous shear stresses

$$d_{\text{TV,max}} = A_2 (\varepsilon^{-1} \eta_o^{-1/2} \rho_c^{-1/2} \sigma) \quad (1.128)$$

where the constant $A_2 \approx 4$ and η_o is the viscosity of the medium.

Equation (1.128) is only valid for low viscosity drops. For emulsions with more viscous drops dispersed in a medium of arbitrary viscosity, $d_{\text{TV,max}}$ is given by the following general expression [89–93]:

$$d_{\text{TX,max}} = A_3 \left(1 + A_4 \frac{\eta_{\text{dr}} \varepsilon^{1/3} d_{\text{TV,max}}^{1/3}}{\sigma} \right)^{3/5} d_k \quad (1.129)$$

where A_3 and A_4 are constants and η_{dr} is the viscosity of the dispersed liquid drops.

The results of experimental investigations of the dependence of droplet size on the determining factors for the TI regime confirm the validity of Eq. (1.30) with $A_1 = 0.86$. This is shown in Figure 1.68 for hexadecane-in-water emulsions using different emulsifiers, where $d_{\text{TI,max}}$ is plotted versus d_k . Comparison of experimental results with theory for TV regime is shown in Figure 1.69 for a large number of emulsions again confirming the validity of Eq. (1.129).

The above analysis is focused on the final equilibrium state of the droplets. However, the kinetics of the breakup process is also of great interest. This kinetic

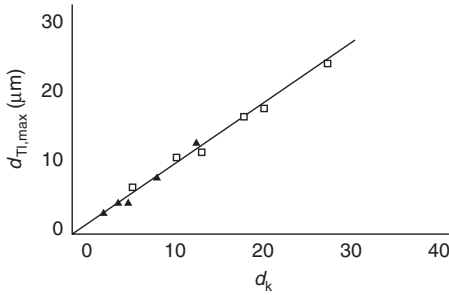


Figure 1.68 Dependence of the maximum droplet diameter $d_{Tl,max}$ (micrometer) in turbulent inertial regime on the determining factor d_k predicted by Eq. (1.32) for emulsions with different emulsifiers.

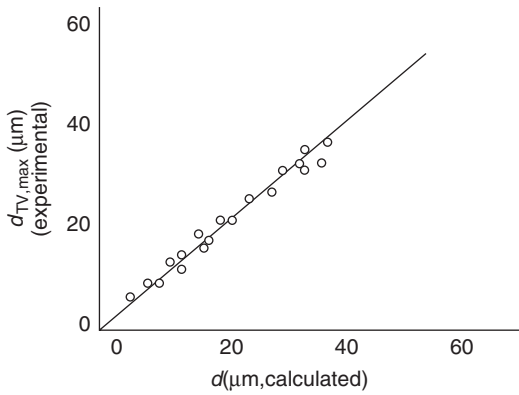


Figure 1.69 Comparison of experimental and theoretical dependence of the maximum droplet diameter $d_{TV,max}$ (micrometer) in turbulent regime on the calculated d predicted by Eq. (1.129) for different emulsions.

process was considered by Vankova *et al.* [94] who introduced a single additional constant k_{dr} that depends on droplet diameter d

$$k_{dr}(d) = B_1 \frac{\varepsilon^{1/3}}{d^{2/3}} \exp \left[-B_2 \left(\frac{d_k}{d} \right)^{5/3} \left(1 + B_3 \frac{\eta_{dr} \varepsilon^{1/3} d^{1/3}}{\sigma} \right) \right] \quad (1.130)$$

where B_1 , B_2 , and B_3 are fitting constants.

The experiments carried out on different emulsions confirmed the validity of Eq. (1.33) and allowed Vankova *et al.* [94] to calculate the values of the constants in Eq. (1.33).

It should be mentioned that the breakup of drops in the flow of emulsions leads to the formation of a large number of droplets with different sizes. The emulsion should be characterized by its maximum size as well as its size distribution. In most cases, the size distribution is represented by a Gaussian function but the real droplet size distribution depends on the viscosity of the droplets [95].

References

1. Tadros, Th.F. and Vincent, B. (1983) in *Encyclopedia of Emulsion Technology* (ed. P. Becher), Marcel Dekker, New York.
2. Binks, B.P. (ed.) (1998) *Modern Aspects of Emulsion Science*, The Royal Society of Chemistry Publication.
3. Tadros, T. (2005) *Applied Surfactants*, Wiley-VCH Verlag GmbH, Germany.
4. Hamaker, H.C. (1937) *Physica (Utrecht)*, **4**, 1058.
5. Deryaguin, B.V. and Landua, L. (1941) *Acta Physicochem. USSR*, **14**, 633.
6. Verwey, E.J.W. and Overbeek, J.Th.G. (1948) *Theory of Stability of Lyophobic Colloids*, Elsevier, Amsterdam.
7. Napper, D.H. (1983) *Polymeric Stabilisation of Dispersions*, Academic Press, London.
8. Walstra, P. and Smolders, P.E.A. (1998) in *Modern Aspects of Emulsions* (ed. B.P. Binks), The Royal Society of Chemistry, Cambridge.
9. Stone, H.A. (1994) *Ann. Rev. Fluid Mech.*, **226**, 95.
10. Wierenga, J.A., van Dieren, F., Janssen, J.J.M., and Agterof, W.G.M. (1996) *Trans. Inst. Chem. Eng.*, **74-A**, 554.
11. Levich, V.G. (1962) *Physicochemical Hydrodynamics*, Prentice-Hall, Englewood Cliffs, NJ.
12. Davis, J.T. (1972) *Turbulent Phenomena*, Academic Press, London.
13. Lucassen-Reynders, E.H. (1996) in *Encyclopedia of Emulsion Technology* (ed. P. Becher), Marcel Dekker, New York.
14. Graham, D.E. and Phillips, M.C. (1979) *J. Colloid Interface Sci.*, **70**, 415.
15. Lucassen-Reynders, E.H. (1994) *Colloids Surf.*, **A91**, 79.
16. Lucassen, J. (1981) in *Anionic Surfactants* (ed. E.H. Lucassen-Reynders), Marcel Dekker, New York.
17. van den Tempel, M. (1960) *Proc. Int. Congr. Surf. Act.*, **2**, 573.
18. Griffin, W.C. (1949) *J. Cosmet. Chem.*, **1**, 311; (1954) **5**, 249.
19. Davies, J.T. (1959) *Proc. Int. Congr. Surf. Act.*, **1**, 426.
20. Davies, J.T. and Rideal, E.K. (1961) *Interfacial Phenomena*, Academic Press, New York.
21. Shinoda, K. (1967) *J. Colloid Interface Sci.*, **25**, 396.
22. Shinoda, K. and Saito, H. (1969) *J. Colloid Interface Sci.*, **30**, 258.
23. Beerbower, A. and Hill, M.W. (1972) *Am. Cosmet. Perfum.*, **87**, 85.
24. Hildebrand, J.H. (1936) *Solubility of Non-electrolytes*, 2nd edn, Reinhold, New York.
25. Hansen, C.M. (1967) *J. Paint Technol.*, **39**, 505.
26. Barton, A.F.M. (1983) *Handbook of Solubility Parameters and Other Cohesive Parameters*, CRC Press, New York.
27. Israelachvili, J.N., Mitchell, J.N., and Ninham, B.W. (1976) *J. Chem. Soc., Faraday Trans. 2*, **72**, 1525.
28. Tadros, Th.F. (1967) in *Solid/Liquid Dispersions* (ed. Th.F. Tadros), Academic Press, London.
29. Batchelor, G.K. (1972) *J. Fluid Mech.*, **52**, 245.
30. Buscall, R., Goodwin, J.W., Ottewill, R.H., and Tadros, Th.F. (1982) *J. Colloid Interface Sci.*, **85**, 78.
31. Tadros, T. (2010) *Rheology of Dispersions*, Wiley-VCH Verlag GmbH, Germany.
32. (a) Asakura, S. and Osawa, F. (1954) *J. Phys. Chem.*, **22**, 1255; (b) Asakura, S. and Osawa, F. (1958) *J. Polym. Sci.*, **33**, 183.
33. Smoluchowski, M.V. (1927) *Z. Phys. Chem.*, **92**, 129.
34. Fuchs, N. (1936) *Z. Phys.*, **89**, 736.
35. Reerink, H. and Overbeek, J.Th.G. (1954) *Discuss. Faraday Soc.*, **18**, 74.
36. Thompson, W. (Lord Kelvin) (1871) *Philos. Mag.*, **42**, 448.
37. Lifshitz, I.M. and Slesov, V.V. (1959) *Sov. Phys. JETP*, **35**, 331.
38. Wagner, C. (1961) *Z. Electrochem.*, **35**, 581.
39. Kabanov, A.S. and Shchukin, E.D. (1992) *Adv. Colloid Interface Sci.*, **38**, 69.
40. Kabanov, A.S. (1994) *Langmuir*, **10**, 680.
41. Weers, J.G. (1998) in *Modern Aspects of Emulsion Science* (ed. B.P. Binks), Royal Society of Chemistry Publication, Cambridge.
42. Deryaguin, B.V. and Scherbaker, R.L. (1961) *Kolloidn. Zh.*, **23**, 33.

43. Friberg, S., Jansson, P.O., and Cederberg, E. (1976) *J. Colloid Interface Sci.*, **55**, 614.
44. Criddle, D.W. (1960) The viscosity and viscoelasticity of interfaces, in *Rheology*, vol. 3, Chapter 11 (ed. F.R. Eirich), Academic Press, New York.
45. Edwards, D.A., Brenner, H., and Wasan, D.T. (1991) *Interfacial Transport Processes and Rheology*, Butterworth-Heinemann, Boston, MA, London.
46. Prince, A., Arcuri, C., and van den Tempel, M. (1967) *J. Colloid Interface Sci.*, **24**, 811.
47. Biswas, B. and Haydon, D.A. (1963) *Proc. Roy. Soc.*, **A271**, 296; (1963) **A2**, 317; Biswas, B. and Haydon, D.A. (1962) *Kolloidn. Zh.*, **185**, 31; (1962) **186**, 57.
48. Tadros, Th.F. (1991) Rheological properties of emulsion systems, in *Emulsions — A Fundamental and Practical Approach*, NATO ASI Series, Vol. **363** (ed. J. Sjöblom), Kluwer Academic Publishers, London.
49. Tadros, Th.F. (1994) *Colloids Surf.*, **A91**, 215.
50. Einstein, A. (1906) *Ann. Physik.*, **19**, 289; (1911) **34**, 591.
51. Bachelor, G.K. (1977) *J. Fluid Mech.*, **83**, 97.
52. Krieger, I.M. and Dougherty, T.J. (1959) *Trans. Soc. Rheol.*, **3**, 137.
53. Krieger, I.M. (1972) *Adv. Colloid Interface Sci.*, **3**, 111.
54. Pal, R. (2000) *J. Colloid Interface Sci.*, **225**, 359.
55. Phan-Thien, N. and Pharm, D.C. (1997) *J. Non-Newtonian Fluid Mech.*, **72**, 305.
56. Pal, R. (2001) *J. Rheol.*, **45**, 509.
57. Mason, T.G., Bibette, J., and Weitz, D.A. (1996) *J. Colloid Interface Sci.*, **179**, 439.
58. Derkach, S.R. (2009) *Adv. Colloid Interface Sci.*, **151**, 1.
59. Saiki, Y., Horn, R.G., and Prestidge, C.A. (2008) *J. Colloid Interface Sci.*, **320**, 569.
60. Princen, H.M. (1986) *Langmuir*, **2**, 519.
61. Lacasse, M.D., Grest, C.S., Levine, D., Mason, T.G., and Weitz, D.A. (1996) *Phys. Rev. Lett.*, **76**, 3448.
62. Mason, T.G., Lacasse, M.D., Grest, C.S., Levine, D., Bibette, J., and Weitz, D.A. (1997) *Phys. Rev. E*, **56**, 3150.
63. Mason, T.G. (1999) *Curr. Opin. Colloid Interface Sci.*, **4**, 231.
64. Babak, V.C. and Stebe, M.J. (2002) *J. Dispersion Sci. Technol.*, **23**, 1.
65. Princen, H.M. and Kiss, A.D. (1986) *J. Colloid Interface Sci.*, **112**, 427.
66. Ponton, A., Clement, P., and Grossiord, J.L. (2001) *J. Rheol.*, **45**, 521.
67. Zao, G. and Chen, S.B. (2007) *J. Colloid Interface Sci.*, **316**, 858.
68. Masalova, I. (2007) *Colloids J.*, **69**, 185.
69. Pal, R. (1996) *AICHE J.*, **42**, 3181.
70. Taylor, G.I. (1934) *Proc. R. Soc. London, Ser. A*, **146**, 501.
71. Choi, C.J. and Schowalter, W.R. (1975) *Phys. Fluids*, **18**, 420.
72. Palierne, J.F. (1990) *Rheol. Acta*, **29**, 204.
73. Doi, M. and Ohta, T. (1991) *J. Chem. Phys.*, **95**, 1242.
74. Bousmina, M. (1999) *Rheol. Acta*, **38**, 73.
75. Grmela, M., Bousmina, M., and Palierne, J.F. (2000) *Rheol. Acta*, **40**, 560.
76. Bousmina, M., Grmela, M., and Palierne, J.F. (2002) *Rheol. Acta*, **46**, 1381.
77. Bousmina, M., Grmela, M., and Zhou, Ch. (2002) *J. Rheol.*, **46**, 1401.
78. Maffettone, P.L. and Minale, M. (1998) *J. Non-Newtonian Fluid Mech.*, **78**, 227.
79. Wetzal, E.D. and Tucker, C.L. (2001) *J. Fluid Mech.*, **426**, 199.
80. Jackson, N.E. and Tucker, C.L. (2003) *J. Rheol.*, **47**, 659.
81. Torza, S., Cox, R.G., and Mason, S.G. (1972) *J. Colloid Interface Sci.*, **38**, 395.
82. Li, X. and Sarker, K. (2005) *J. Rheol.*, **49**, 1377.
83. Hinch, T.J. and Arcivos, A. (1980) *J. Fluid Mech.*, **98**, 305.
84. Grace, H.P. (1982) *Chem. Eng. Commun.*, **14**, 225.
85. Renardly, Y. (2008) *Rheol. Acta*, **47**, 89.
86. Mason, T.G. and Bibette, J. (1996) *J. Phys. Rev. Lett.*, **77**, 3481.
87. Heinze, J.O. (1955) *AICHE J.*, **1**, 289.
88. Vankova, N., Tcholakova, S., Denkov, N.D., Ivanov, I.B., Vulchev, V.D., and Danner, Th. (2007) *J. Colloid Interface Sci.*, **312**, 363.
89. Podgorska, W. (2006) *Chem. Eng. Sci.*, **61**, 2986.

90. Calabrese, R.V., Chang, T.P.K., and Dang, P.T. (1986) *AICHE J.*, **32**, 657.
91. Wang, C.Y. and Calabrese, R.V. (1986) *AICHE J.*, **32**, 677.
92. Razzaque, M.M., Afacan, A., Lu, Sh., Nandakumar, K., Jacob, H., Masliyah, J.H., and Sanders, R.S. (2003) *Int. J. Multiphase Flow*, **29**, 1451.
93. Eastwood, C.D., Armi, L., and Lasheras, J.C. (2004) *J. Fluid Mech.*, **502**, 309.
94. Vankova, N., Tcholakova, S., Denkov, N.D., and Danner, Th. (2007) *J. Colloid Interface Sci.*, **313**, 612.
95. Tcholakova, S., Vankova, N., Denkov, N.D., and Danner, Th. (2007) *J. Colloid Interface Sci.*, **310**, 570.

